

Syntheses and photophysical properties of diaminotetraphenylporphyrins and their corresponding polyimides

Sudkanueng Singto^a, Supawan Tantayanon^{b, **}, Christopher A. Zoto^{c, *},
Robert E. Connors^c

^a Graduate Program of Petrochemistry, Faculty of Science, Chulalongkorn University, Bangkok, 10330, Thailand

^b Green Chemistry Research Laboratory, Department of Chemistry, Faculty of Science, Chulalongkorn University, Bangkok, 10330, Thailand

^c Department of Chemistry and Biochemistry, Worcester Polytechnic Institute, Worcester, MA, USA

ARTICLE INFO

Article history:

Received 30 July 2017

Received in revised form

24 September 2017

Accepted 25 September 2017

Available online 26 September 2017

Keywords:

Porphyrin
Polyimide
Absorption
Fluorescence
Quenching
Stern-Volmer

ABSTRACT

Two free base porphyrins, 5,10-bis(4-aminophenyl)-15,20-diphenylporphyrin (*cis*-DATPP), 5,15-bis(4-aminophenyl)-10,20-diphenylporphyrin (*trans*-DATPP), and their zinc metalated analogues (*cis*-ZnDATPP and *trans*-ZnDATPP) were synthesized. A series of their corresponding polyimides were obtained by the condensed polymerization of the respective monomeric isomer DATPP with a 1:1 ratio of 2,2'-bis(trifluoromethyl)-4,4'-diaminobiphenyl (PFMB) and 4,4'-hexafluoroisopropylidenediphthalic anhydride (6FDA). The inclusion of PFMB and 6FDA into the polymeric backbone causes the polymers to be moderately to highly soluble in organic polar solvents. The molar content of the respective DATPP monomer varied between 5 and 30%. All compounds were structurally characterized by ¹H NMR and ATR-IR spectroscopy and the porphyrin content in the polyimides was determined by UV–Visible absorption spectroscopy. Photophysical properties consisted of measuring both the UV–Visible (ground state) absorption and fluorescence (excited state) spectra, fluorescence quantum yields (Φ_f), and fluorescence lifetimes (τ_f) in dichloromethane and N,N-dimethylacetamide. Fluorescence quenching was also measured and observed by the Stern-Volmer relationship, using 9,10-anthraquinone (AQ) as the quencher molecule. Both the bimolecular rate constant of fluorescence quenching (k_q) and the Stern-Volmer constant (K_Q) were calculated from this relationship. Furthermore, deviations from linearity depicted in the Stern-Volmer plots for TPP and ZnTPP at higher concentrations of AQ were also measured as a means of examining and explaining the simultaneous occurrence of dynamic (collisional) quenching and static quenching in the mechanisms of fluorescence quenching. It was found in this work that the significantly larger values in the static quenching constant (K_S) than in the dynamic quenching constant (K_D) are indicative that static quenching and ground state complex formation between the fluorophore and quencher is the dominant mechanism of fluorescence quenching of these systems at higher quencher concentrations.

© 2017 Elsevier B.V. All rights reserved.

1. Introduction

Porphyrins and polyimides are two classes of organic compounds that have attracted much interest in a wide variety of applications, ranging in their use as photosensitizers in different types of electron and energy transfer processes, water purification, novel chemical synthesis and catalysis, artificial solar energy conversion

(photovoltaic) systems, and many more [1–28]. Much attention has been focused on the synthesis of aromatic polyimides containing porphyrin moieties within the polymer backbone chain for studying their fundamental spectroscopic and photophysical properties in applications of artificial solar energy conversion systems [22,23], catalysts [24], photoresponsive materials [25], molecular wires [26], and photoinduced intramolecular electron transfer properties [19–21,27]. The presence and covalent attachment of porphyrin units in the polyimide backbone chain introduces the following three chemical characteristics: (1) higher degree of aromaticity, (2) extended π -conjugation, and (3) higher degree of electron donating behavior. These three characteristics are expected to result in an

* Corresponding author.

** Corresponding author.

E-mail address: czoto@hotmail.com (C.A. Zoto).

enhancement in the photoinduced intramolecular charge transfer properties of these compounds, in that photon absorption results in the transfer of electronic charge from the electron donor end of the molecule (porphyrin moiety) to the electron acceptor end of the molecule (electron withdrawing moieties along the polyimide backbone chain). Furthermore, in addition to the characteristics mentioned, the presence of electron donating porphyrin groups introduces unique absorbance and fluorescence spectral properties in the visible region of the electromagnetic spectrum.

Porphyrins are tetrapyrrolic macrocyclic compounds that belong to the family of organic compounds called porphyrinoids. Fig. 1 shows the chemical structures of porphyrin and meso-5,10,15,20-tetraphenylporphyrin (TPP). A single porphyrin macrocycle is nominally composed of 22 π electrons, 18 of which belong to the π -conjugated delocalization framework. A generic porphyrin backbone is structurally composed of four 'pyrrole-type' rings covalently linked together by four methine bridging groups to give an aromatically conjugated macrocyclic ring consisting of a sp^2 hybridized framework [1,2]. Porphyrins are known for their characteristic red and purple colors both in their solid and solution states and are efficient chromophores. Free base (or nonmetallated) porphyrins generally show four weak absorption bands, known as Quasi, or Q, bands in the visible absorption spectrum at an approximate wavelength range between 500 and 650 nm and a strongly intense absorption band in the near-UV region called the Soret, or S, band appearing at a wavelength of around 400 nm, characteristic with the π -conjugation of the macrocyclic ring [2,3]. Porphyrins are also recognized for their strongly intense fluorescence properties and their higher degree of π -conjugation makes them more red shifted fluorophores [4–11].

Porphyrins have been used in a wide variety of applications ranging in their use as photosensitizers for different types of electron, electron energy transfer, and energy storage processes, water purification, novel chemical synthesis, and decontamination of chemical and biological materials [12–14]. In particular, porphyrins are commonly used photosensitizers for singlet state oxygen ($^1\Delta_g$), a reactive oxygen species that has found widespread attention as a

cytotoxic agent in photodynamic therapy (PDT) in destroying targeted tumor and cancerous cells in living organisms [15]. Additionally, singlet oxygen has been used as a reactive intermediate in the photooxidation of organic compounds in solution because of its high chemical energy content and its low lying excited states [16,17]. Aromatic polyimides are a class of organic compounds traditionally synthesized by the treatment of an aromatic diamine with an aromatic tetracarboxylic acid dianhydride [18] known for their thermal stability, high softening temperatures, chemical resistance, and mechanical properties [19–21,28]. Dianhydrides are reported as good electron acceptor groups and diamines are good electron donor groups, which thereby cause polyimides to easily form a charge transfer complex between the electron donor and acceptor groups [28].

The work presented in this manuscript reports on the direct syntheses of two free base monomeric porphyrin isomers, namely 5,10-bis(4-aminophenyl)-10,20-diphenylporphyrin (*cis*-DATPP) and 5,15-bis(4-aminophenyl)-10,20-diphenylporphyrin (*trans*-DATPP), their zinc metalated analogues, and their corresponding polyimides (see Fig. 2 for the chemical structures of *cis*-DATPP and *trans*-DATPP). The photophysical properties of these compounds were investigated, which involved measuring the UV–Visible (ground state) absorption spectra, fluorescence (excited state) spectra, fluorescence quantum yields (Φ_f), and fluorescence lifetimes (τ_f) in N,N-dimethylacetamide and dichloromethane. The fluorescence quenching of these classes of organic compounds were investigated in the presence of 9,10-anthraquinone (see Fig. 3) as the quencher compound using the Stern-Volmer relationship. The effects that polymerization, polymer molecular weights, and weight percent of porphyrin content in the polymers have on the photophysical properties of these class of compounds are discussed in the manuscript. Furthermore, the work presented in this manuscript will provide important information into the syntheses and photophysical properties of these classes of organic compounds. A thorough understanding of the properties of these compounds is pertinent to examining their applications.

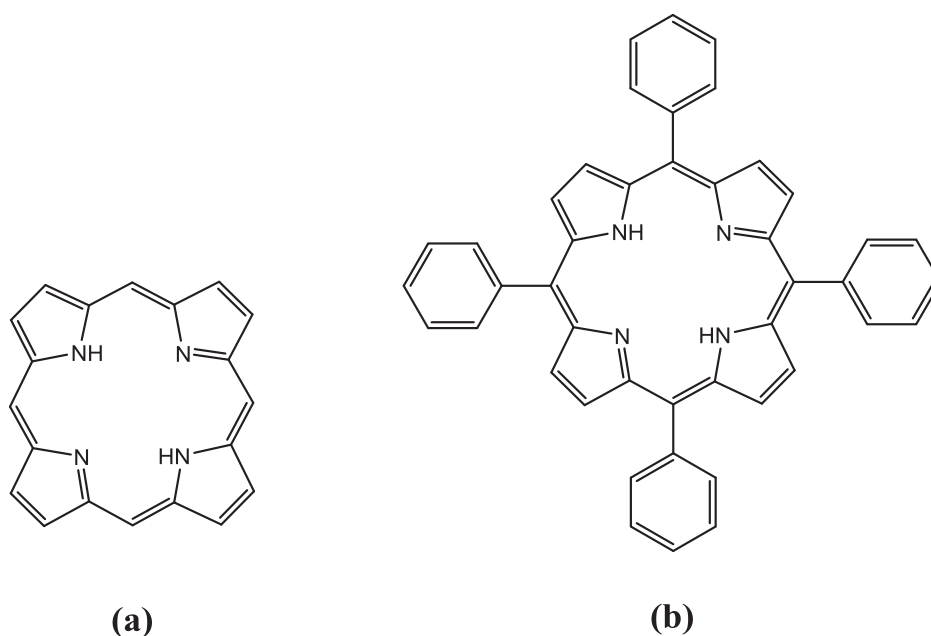


Fig. 1. Chemical structures of (a) porphyrin (porphine) and (b) meso-5,10,15,20-tetraphenylporphyrin (TPP).

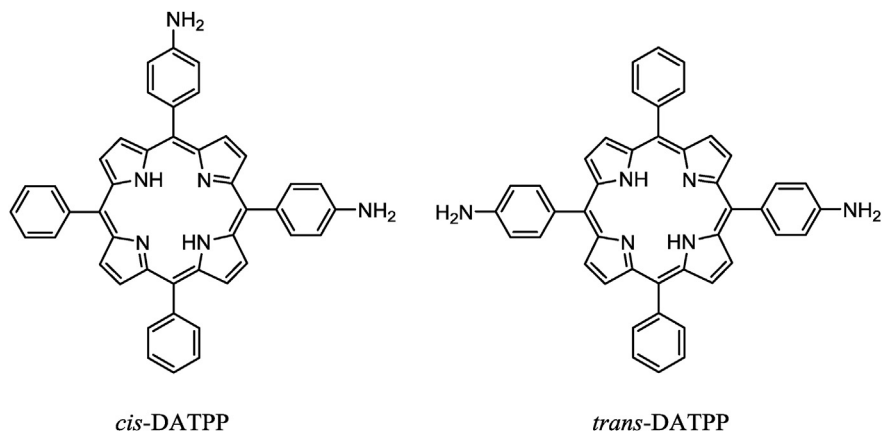


Fig. 2. Chemical structures of 5,10-bis(4-aminophenyl)-10,20-diphenylporphyrin (*cis*-DATPP) and 5,15-bis(4-aminophenyl)-10,20-diphenylporphyrin (*trans*-DATPP).

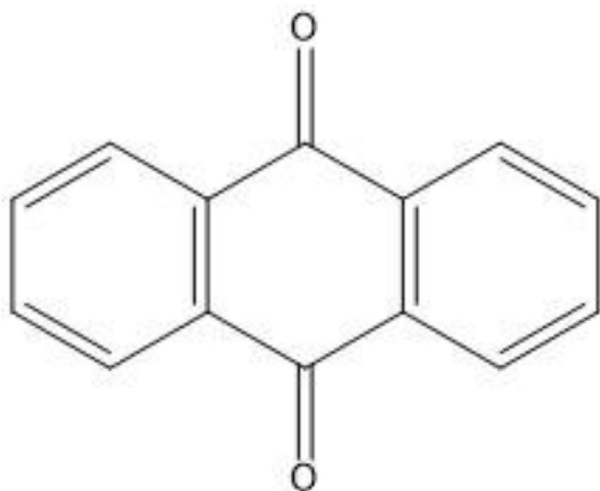


Fig. 3. Chemical structure of 9,10-anthraquinone.

2. Experimental

2.1. Chemical reagents and solvents

All chemical reagents and solvents were purchased from Sigma-Aldrich, Acros Organics, Fluka, Fisher Scientific, EMD, Alfa Aesar, and Merck. All reagents and solvents not mentioned in the following paragraph were used without further purification.

Purification workup was done for the following materials prior to use: 9,10-anthraquinone was sublimed, benzaldehyde was distilled under reduced pressure, pyrrole was distilled over calcium hydride under reduced pressure. Dichloromethane was distilled over calcium hydride, and N-methyl-2-pyrrolidone was distilled over calcium hydride. Compound 2,2'-bis(trifluoromethyl)-4,4'-diaminobiphenyl (PFMB) was obtained from Dr. Frank W. Harris's research lab at the University of Akron in Ohio.

2.2. Instrumentation

Proton Nuclear Magnetic Resonance (^1H NMR) spectra were obtained in chloroform- d (CDCl_3) or dimethyl sulfoxide- d_6 ($\text{DMSO}-d_6$) using a Bruker[®] AVANCE 400 MHz NMR spectrometer. Chemical shifts (δ) are reported in parts per million (ppm) relative to the residual protonated solvent signal as a reference. Attenuated Total

Reflectance Infrared spectra (ATR-IR) were measured on a Perkin Elmer[®] Spectrum One IR spectrometer. The molecular weights of all polyimides were determined by Gel Permeation Chromatography (GPC) using a Waters[®] 150-CV chromatography system. UV–Visible absorption spectra were measured on a Perkin Elmer[®] Lambda 35 UV/VIS spectrometer. Fluorescence spectra were measured using a Perkin Elmer[®] LS 50B spectrophotometer.

2.3. Chemical syntheses and structural characterization data

Presented in this section are the synthetic procedures, reaction schemes, and spectral characterization data (^1H NMR and ATR-IR) of all target compounds.

2.3.1. Meso-5,10,15,20-tetraphenylporphyrin (TPP)

Meso-5,10,15,20-tetraphenylporphyrin (TPP) was synthesized from the acid catalyzed condensation of pyrrole (4 mol eq.) and benzaldehyde (4 mol eq.) in the presence of propionic acid [29]. Benzaldehyde (1.62 mL, 16 mmol) and pyrrole (1.11 mL, 16 mmol) were combined and heated under reflux in the presence of propionic acid (100 mL). The reaction mixture was refluxed for 1 h, followed by stirring for 30 min at ambient room temperature. Cold methanol (20 mL) was added and the mixture was continuously stirred in an ice bath. The product was filtered off, then washed with hot water and methanol until the filtrate was colorless, affording purple glistening crystals. Fig. 4a shows the reaction scheme for the synthesis of TPP. Yield: 0.21 g, 27%. Melting point: >400 °C. ^1H NMR (CDCl_3): δ (ppm) -2.73 (s, 2H, internal NH), 7.28 (s, 4H, *p*-phenyl), 7.79 (m, 12H, *m*- and *p*-phenyl), 8.24–8.21 (m, 8H, *o*-phenyl), 8.88 (s, 8H, β -pyrrole). ATR-IR (cm^{-1}): 3314 (NH), 3050 and 3017 (ArH), 1470 and 1440 (NH bending), 698 (out of plane bending deformation, monosubstituted benzene).

2.3.2. Zinc(II) 5,10,15,20-tetraphenylporphyrin (ZnTPP)

To a boiling solution of TPP (0.76 g, 1.24 mmol) in chloroform (150 mL) was added a saturated solution of zinc acetate dihydrate (0.40 g, 1.86 mmol) in methanol (3 mL). The reaction mixture was heated under reflux for 30 min, cooled down to room temperature, and extracted twice with distilled water. The organic layer was dried over anhydrous sodium sulfate and filtered off. Purple crystals were collected by filtration and washed with cold methanol [29]. Fig. 4b shows the reaction scheme for the synthesis of ZnTPP. Yield: 0.83 g, 99%. Melting point: >400 °C. ^1H NMR (CDCl_3): δ (ppm) 7.23 (s, 4H, *p*-phenyl), 7.69–7.64 (m, 12H, *m*- and *p*-phenyl), 8.16–8.09

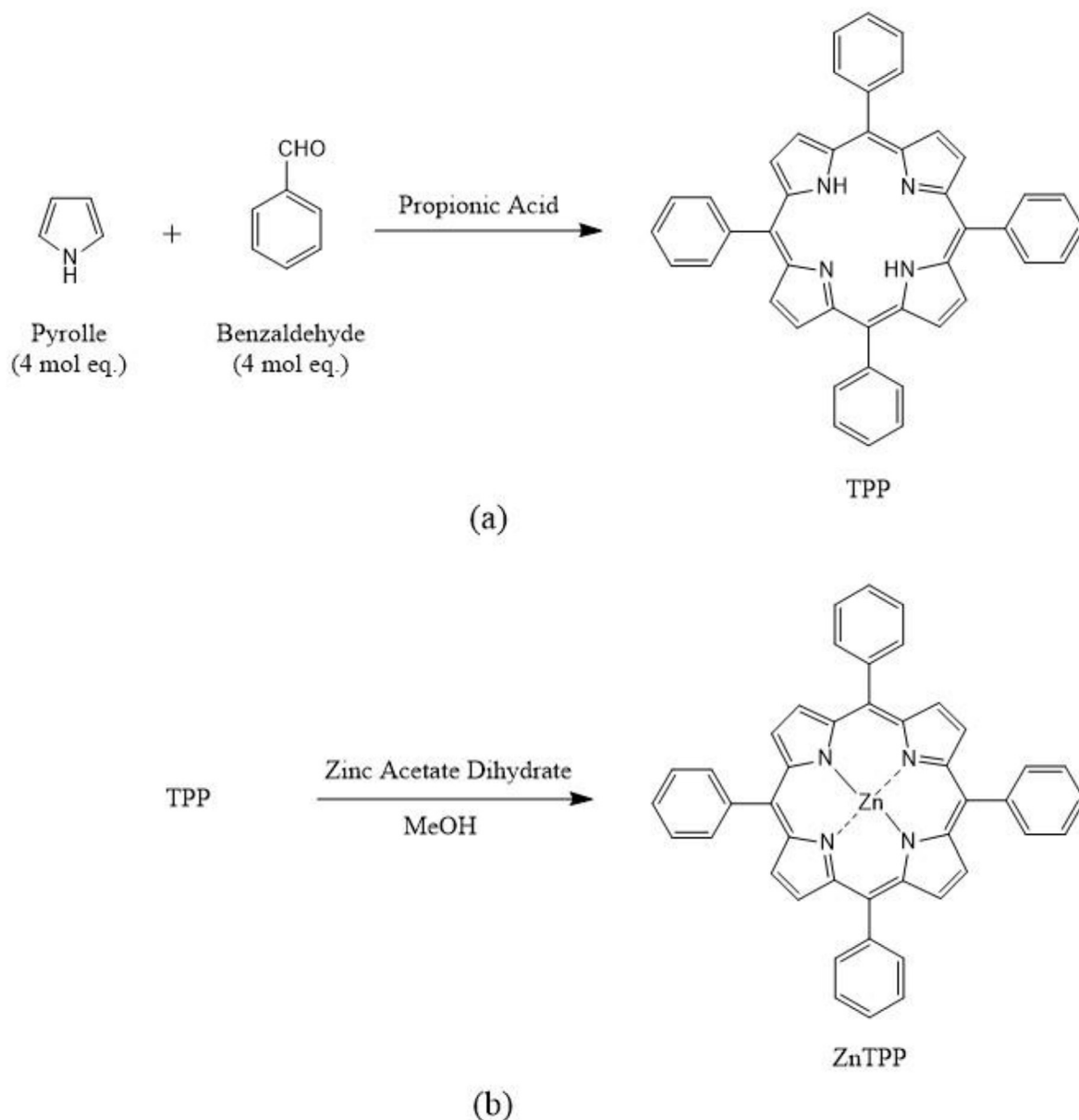


Fig. 4. Reaction schemes for the syntheses of (a) TPP and (b) ZnTPP.

(m, 8H, *o*-phenyl), 8.84 (s, 8H, β -pyrrole). ATR-IR (cm^{-1}): 1593, 1480, 1440, 1340, 1000, 797, 751. When directly compared to free base TPP, the signal at $\delta -2.73$ ppm (representing the internal N–H protons) disappears, as well as the absorption band at 3314 cm^{-1} in the IR spectrum, indicative to porphyrin metalation.

2.3.3. 5,10-bis(4-aminophenyl)-10,20-diphenylporphyrin (*cis*-DATPP) and 5,15-bis(4-aminophenyl)-10,20-diphenylporphyrin (*trans*-DATPP)

Both *cis*-DATPP and *trans*-DATPP were synthesized using the approach formulated by Raymond et al. [30]. Fig. 5 shows the two step reaction scheme for the syntheses of *cis*-DATPP and *trans*-DATPP. To a solution of meso-5,10,15,20-tetraphenylporphyrin (200 mg, 0.33 mmol) in trifluoroacetic acid (10 mL) was added sodium nitrite (183 mg, 2.65 mmol). After 90 s of continuous stirring at ambient room temperature, the reaction was poured into water (100 mL) and extracted with dichloromethane (6×25 mL).

The residue obtained was purified as described above and then reduced using tin(II) chloride dihydrate (0.80 g, 3.55 mmol) in concentrated hydrochloric acid (50 mL). The reaction was heated under reflux to 65°C for 90 min, followed by cooling the solution to ambient room temperature, pouring it into ice water and adjusting to pH 8 with concentrated ammonium hydroxide. The aqueous phase was extracted with dichloromethane (5×100 mL), and the combined organic layer extracts were dried over anhydrous magnesium sulfate. The organic phase was concentrated *in vacuo* and the solution was pre-absorbed onto silica gel. Silica gel flash column chromatography using a gradient mixture of dichloromethane and ethyl acetate afforded first *trans*-DATPP, followed by *cis*-DATPP. Each regioisomer was recrystallized from methanol, yielding 32% of *cis*-DATPP and 28% of *trans*-DATPP. Fig. 5 shows the reaction scheme for the preparations of *cis*-DATPP and *trans*-DATPP. *cis*-DATPP: $^1\text{H NMR}$ (DMSO-d_6): δ (ppm) -2.83 (s, 2H, internal NH), 5.48 (s, 4H, NH_2), 6.93 (d, 4H, aminophenyl), 7.69–7.80 (m, 10H, phenyl), 8.08 (d, 4H, aminophenyl), 8.69 (s, 4H, β -H), 8.86 (s, 4H, β -

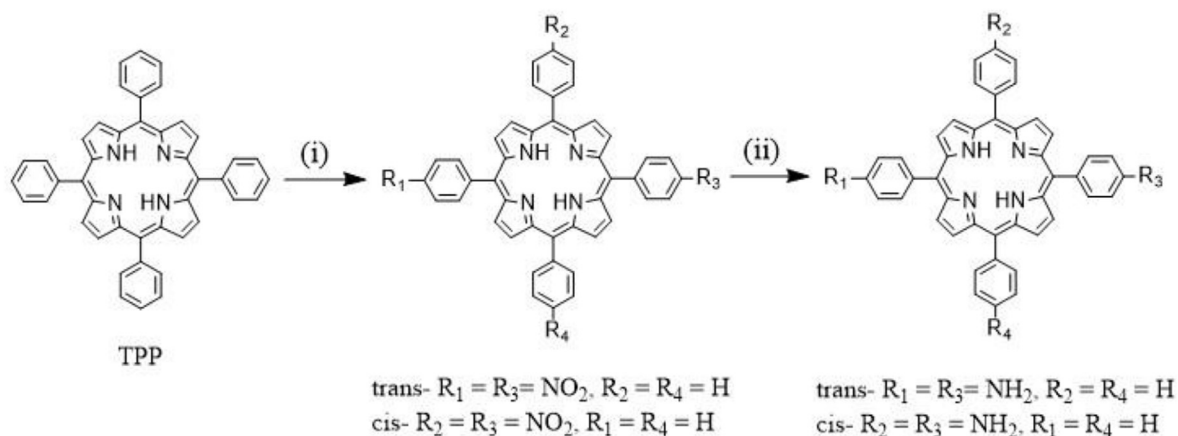


Fig. 5. Reaction scheme for the syntheses of *cis*-DATPP and *trans*-DATPP. (i) Sodium nitrite (NaNO_2) and trifluoroacetic acid (TFA); (ii) Tin(II) chloride dihydrate ($\text{SnCl}_2 \cdot 2\text{H}_2\text{O}$), concentrated hydrochloric acid (HCl), heated under reflux to 65°C .

H); ATR-IR (cm^{-1}): 3325 (NH), 1510 (NH), 800 (1,4-substituted phenyl). *trans*-DATPP: ^1H NMR (DMSO-d_6): δ (ppm) -2.81 (s, 2H, internal NH), 5.52 (s, 4H, NH_2), 6.92 (d, 4H, aminophenyl), 7.73–7.78 (m, 10H, phenyl), 8.22 (d, 4H, aminophenyl), 8.70 (d, 4H, β -H), 8.87 (d, 4H, β -H). ATR-IR (cm^{-1}): 3328 (NH), 1504 (NH), 800 (1,4-substituted phenyl).

2.3.4. Zinc(II) 5,10-bis(4-aminophenyl)-10,20-diphenylporphyrin (*cis*-ZnDATPP) and zinc(II) 5,15-bis(4-aminophenyl)-10,20-diphenylporphyrin (*trans*-ZnDATPP)

Both *cis*-ZnDATPP and *trans*-ZnDATPP were synthesized according to Anannarukan et al. [31]. Fig. 6 shows the reaction scheme for the syntheses of *cis*-ZnDATPP and *trans*-ZnDATPP. The respective free base DATPP regioisomer was used as the starting compound for the synthesis of the zinc metalated derivative. A solution composed of *cis*-DATPP or *trans*-DATPP (638 mg, 0.99 mmol) and zinc acetylacetonate dihydrate (1.28 g, 4.53 mmol) in tetrahydrofuran (190 mL) was heated under reflux for 4 h. The product mixture was concentrated *in vacuo* and the resulting precipitate was recrystallized from methanol to afford violet crystals. *cis*-ZnDATPP: Yield: 0.56 g, 80%. Melting point $>300^\circ\text{C}$. ^1H NMR (DMSO-d_6): δ (ppm) 5.53 (s, 4H, NH_2), 6.93 (d, 4H, aminophenyl),

7.68–7.85 (m, 10H, phenyl), 8.13 (d, 4H, aminophenyl), 8.69 (s, 4H, β -H), 8.86 (s, 4H, β -H). ATR-IR (cm^{-1}): 1610, 1481, 1339, 1175, 993, 795. *trans*-ZnDATPP: Yield: 0.66 g, 85%. Melting point $>300^\circ\text{C}$. ^1H NMR (DMSO-d_6): δ (ppm) 5.52 (s, 4H, NH_2), 6.93 (d, 4H, aminophenyl), 7.68–7.79 (m, 10H, phenyl), 8.17 (d, 4H, aminophenyl), 8.70 (d, 4H, β -H), 8.87 (d, 4H, β -H). ATR-IR (cm^{-1}): 1596, 1489, 1178, 992, 795. Similar to the NMR and IR spectral data of ZnTPP, the signals at $\delta \sim -2.8$ ppm (representing the internal N–H protons) disappear, as well as the absorption band at $\sim 3330\text{ cm}^{-1}$ in the IR spectrum, indicative to porphyrin metalation.

2.3.5. Polyimide series

The porphyrin containing polyimides were synthesized according to Anannarukan et al. [31]. Four series of polyimides were prepared for each respective porphyrin diamine monomer (see Table 1). Fig. 7 shows the general reaction scheme for the syntheses of the porphyrin containing polyimide series of compounds. The dianhydride monomer, 4,4'-hexafluoroisopropylidenediphthalic anhydride (6FDA) was added to the respective porphyrin diamine monomer and 2,2'-bis(trifluoromethyl)-4,4'-diaminobiphenyl (PFMB) at various mole % ratios (Table 1) in dry N-methyl-2-pyrrolidone (NMP) containing a small catalytic amount of

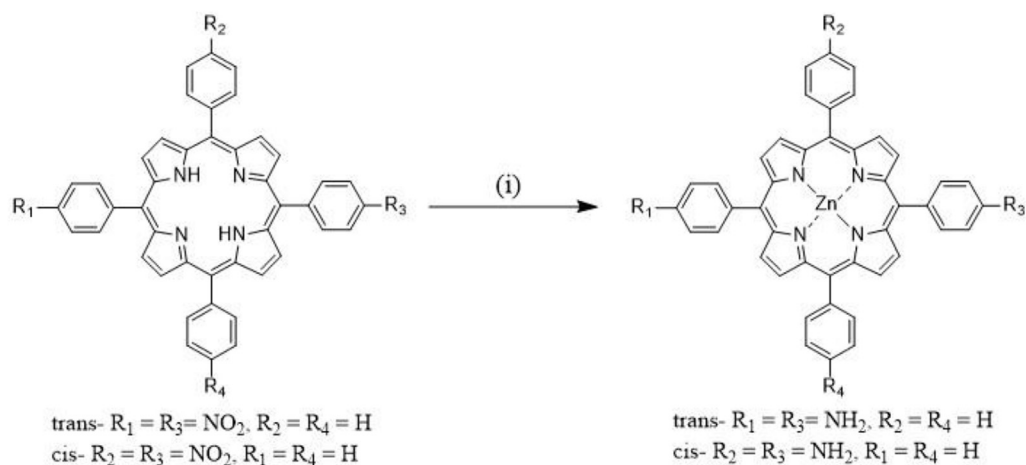


Fig. 6. Reaction scheme for the syntheses of *cis*-ZnDATPP and *trans*-ZnDATPP. (i) Zinc acetylacetonate dihydrate, tetrahydrofuran, heated under reflux for 4 h.

Table 1
Polyimide series I–IV. Various starting mole percent monomer ratios, product percent yields, and product decomposition temperatures.

Series I (from <i>cis</i> -DATPP)					
PI	Mole Percent Monomer Ratios (%)			Percent Yield (%)	Decomposition Temperature (°C)
	6FDA	PFMB	<i>cis</i> -DATPP		
PI-C1	100	95	5	94.88	532
PI-C2	100	90	10	93.53	538
PI-C3	100	85	15	92.22	522
PI-C4	100	70	30	91.14	527
Series II (from <i>trans</i> -DATPP)					
PI	Mole Percent Monomer Ratios (%)			Percent Yield (%)	Decomposition Temperature (°C)
	6FDA	PFMB	<i>trans</i> -DATPP		
PI-T1	100	95	5	92.75	534
PI-T2	100	90	10	92.70	528
PI-T3	100	85	15	91.74	516
PI-T4	100	70	30	89.63	531
Series III (from <i>cis</i> -ZnDATPP)					
PI	Mole Percent Monomer Ratios (%)			Percent Yield (%)	Decomposition Temperature (°C)
	6FDA	PFMB	<i>cis</i> -ZnDATPP		
PI-ZnC1	100	95	5	94.59	521
PI-ZnC2	100	90	10	91.59	518
PI-ZnC3	100	85	15	91.48	513
PI-ZnC4	100	70	30	93.15	520
Series IV (from <i>trans</i> -ZnDATPP)					
PI	Mole Percent Monomer Ratios (%)			Percent Yield (%)	Decomposition Temperature (°C)
	6FDA	PFMB	<i>trans</i> -ZnDATPP		
PI-ZnT1	100	95	5	93.72	510
PI-ZnT2	100	90	10	91.78	519
PI-ZnT3	100	85	15	90.40	516
PI-ZnT4	100	70	30	92.15	522

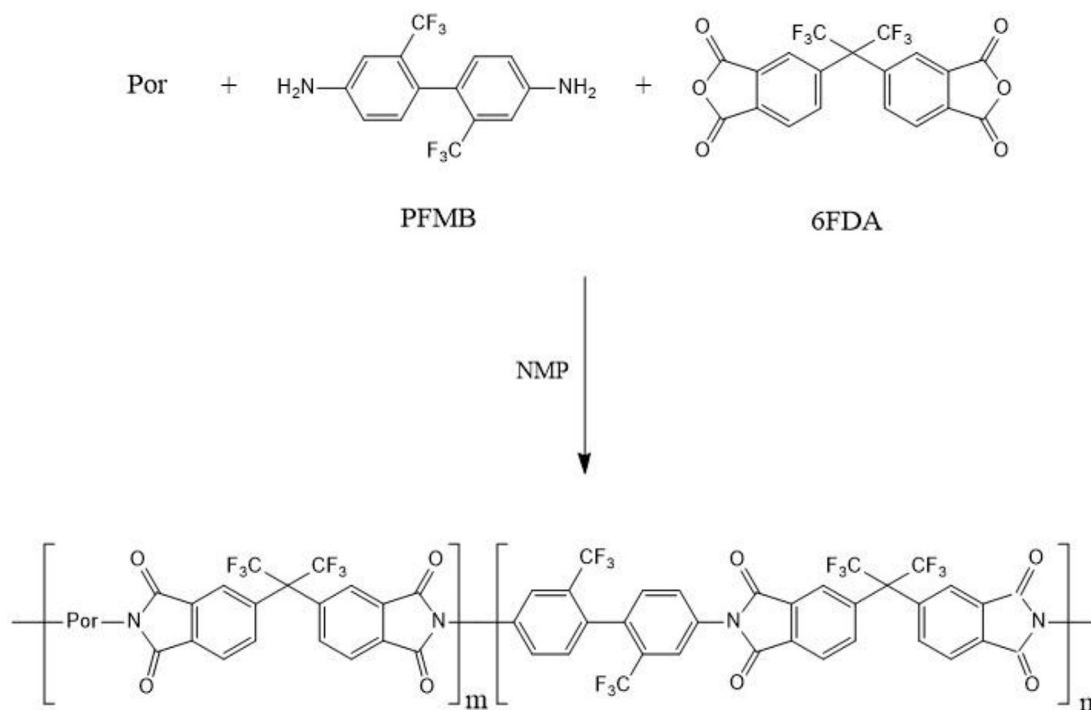


Fig. 7. Reaction scheme for the syntheses of the polyimide series. Por: *cis*-DATPP, *trans*-DATPP, *cis*-ZnDATPP, or *trans*-ZnDATPP.

isoquinoline under nitrogen at ambient room temperature. After the solution was continuously stirred for 8 h, it was heated under reflux and maintained at 220 °C for 12 h. The solution was allowed to cool to ambient room temperature, followed by slowly adding it to vigorously stirred methanol. The resulting precipitated polymer was collected by vacuum filtration, washed with cold methanol, and dried under reduced pressure at 200 °C for 24 h. The polymers were obtained in 89–95% yields.

All polyimide compounds were structurally characterized by ¹H NMR and ATR-IR spectroscopy. The Supplementary Information provides the graphical ¹H NMR and ATR-IR spectra. From the IR characterization data, the absorption band of the amine functional group was not observed, indicating the absence of precursor amine monomer compounds in the polyimide compounds. In addition, no absorption bands of both the amide and carboxylic acid functional groups of the poly(amic acid) intermediate appeared in the spectra, indicating that the poly(amic acid) was completely converted to the corresponding polyimides during the refluxing step. Complete conversion to the polyimides was confirmed by the presence of the absorption bands at 1784 cm⁻¹ (asymmetric stretching C=O), 1728 cm⁻¹ (symmetric stretching C=O), 1365 cm⁻¹ (C–N stretching), and 721 cm⁻¹ (C=O bending), which are the characteristic absorption bands of the polyimide. Polyimides in series I and II containing the free base *cis*- and *trans*-DATPP have the internal N–H group in the porphyrin structure. However, the characteristic N–H absorption band was not observed in the IR spectra and this is potentially attributed to the rigid structure of the polymer backbone chain, making it difficult for N–H vibration to occur. ¹H NMR spectral data of all polyimides shows a signal at δ 8.90 ppm, attributed to the hydrogen atoms located at the β positions on the pyrrole rings of the porphyrin moiety. Polyimides in series I and II containing the free base *cis*- and *trans*-DATPP showed the signal of the internal N–H proton at δ –2.80 ppm, which was not present in the ¹H NMR spectra for the polyimides in series III and IV containing metalated *cis*- and *trans*-ZnDATPP, confirming the occurrence of zinc metalation within the porphyrin macrocycle. Furthermore, ¹H NMR confirmed the incorporation of the porphyrin units in the polymer structure.

2.4. Photophysical and fluorescence quenching measurements

Photophysical properties involved first measuring the UV–Visible absorption spectra and fluorescence spectra of the target compounds in dichloromethane and N,N-dimethylacetamide to obtain the spectral maxima locations. Fluorescence quantum yield (Φ_f) is defined as the fraction of chromophore molecules undergoing fluorescence from the excited singlet state to the ground singlet state, indicating a measure of fluorescence efficiency. Fluorescence quantum yields were determined by comparing the corrected integrated fluorescence spectrum of the sample with that of a known standard using a set of correction factors for the instrument's photomultiplier tube (PMT) detector according to [32]. For the free base porphyrin compounds TPP, *cis*-DATPP, *trans*-DATPP, and their corresponding polyimides, the following standards were used: TPP in toluene (Φ_f = 0.1 ± 0.001) [33], TPP in dichloromethane (Φ_f = 0.116, measured value), and TPP in N,N-dimethylacetamide (Φ_f = 0.15, measured value). For the Zn metalated porphyrinic compounds ZnTPP, *cis*-ZnDATPP, *trans*-ZnDATPP, and their corresponding polyimides, the following standards were used: ZnTPP in toluene (Φ_f = 0.033) [34], ZnTPP in dichloromethane (Φ_f = 0.02, measured value), and ZnTPP in N,N-dimethylacetamide (Φ_f = 0.024, measured value).

Eq. (1) defines Φ_f

$$\Phi_f = \Phi_{f, std} \left(\frac{A_{std}}{A} \right) \left(\frac{n^2}{n_{std}^2} \right) \left(\frac{D}{D_{std}} \right) \quad (1)$$

where A is the absorbance at the excitation wavelength, n is the refractive index of the solvent, and D is the integrated area under the corrected fluorescence spectrum. Solutions of both the standard and sample were prepared initially with the absorbance at λ_{max} approximately equal to 0.5, followed by an accurate tenfold dilution. Fluorescence spectra used to determine Φ_f were corrected with sets of correction factors that were obtained by measuring the spectra of compounds with known emission spectra [32].

Fluorescence lifetime (τ_f) is equal to the time after which the fluorescence intensity of a fluorophore has dropped to 1/e of its initial value after a pulsed excitation (where “e” is the Euler base). In other words, it is a measure of the time a fluorophore spends in the excited singlet state before emitting a photon and returning back to the ground singlet state [17]. Eqs. (2) and (3) define τ_f

$$I(t) = I_0(t) \exp\left(-\frac{t}{\tau_f}\right) \quad (2)$$

$$\tau_f = \frac{1}{k_f + k_{nr}} \quad (3)$$

where I(t) and I₀(t) are the relative fluorescence intensities at time, t, and at time, 0; τ_f is the fluorescence lifetime, k_f is the radiative decay rate constant, and k_{nr} is the nonradiative decay rate constant (k_{nr} = k_{IC} + k_{ISC}).

Fluorescence lifetimes were measured with a Photon Technology International® TM-3 time resolved spectrofluorometer with pulsed nitrogen/dye laser excitation. All solutions were degassed with N₂ to prevent excited state quenching by molecular oxygen. Felix32 analysis module was the computer software program used for generating the time dependent fluorescence decay spectra. Data analysis involved using a curve fitting procedure and best fit curves were chosen on how well the statistically fitted curve overlaid with the sample decay curve. The chi-squared (χ²) value had to lie within the range of 0.9–1.2 for accurate measurements. In addition, the fluorescence decay of an Instrument Response Function (IRF) was measured to be at about the same maximum intensity as that of the sample decay. The IRF used was an aqueous non-dairy creamer solution.

Fluorescence quenching was measured and observed by the Stern-Volmer relationship, using 9,10-anthraquinone as the quencher molecule. The Stern-Volmer relationship is expressed by Eq. (4)

$$\frac{F_0}{F_t} = 1 + K_Q[Q] \quad (4)$$

where F₀ and F_t are the relative fluorescence intensities in the absence and presence of quencher (Q), [Q] is the molar concentration of the quencher, and K_Q is the Stern-Volmer constant (K_Q = τ_fk_q, where τ_f is the fluorescence lifetime in the absence of quencher and k_q is the bimolecular quenching rate constant).

The value of k_q is approximately equal to the diffusion rate constant (k_d), which generally shows the rate which reactant components A and B diffuse together in solution and collide, defined by Eq. (5)

$$k_d = \frac{8000RT}{3\eta} \quad (5)$$

where R is the universal gas constant (8.3145 J mol⁻¹ K⁻¹), T is the absolute temperature, and η is the viscosity of the solvent. The reported viscosities of dichloromethane and N,N-dimethylacetamide are 4.13×10^{-4} kg m⁻¹ s⁻¹ and 1.96×10^{-3} kg m⁻¹ s⁻¹, respectively [35]. Therefore, the k_d values for CH₂Cl₂ and DMAc are 1.57×10^{10} and 3.32×10^9 M⁻¹ s⁻¹, respectively.

Stock solutions of the respective porphyrin monomer remained at a constant molar concentration (5×10^{-6} M). A series of 8×5 mL aliquot solutions were prepared in volumetric flasks, keeping the porphyrin analyte volume (2.5 mL), and hence concentration, constant, in all of the solutions. The molar concentration of 9,10-anthraquinone varied in the range of 2.0×10^{-4} M and 1.4×10^{-3} M (see Table 2).

3. Results and discussion

3.1. UV–visible absorption and fluorescence spectra

The room temperature UV–Visible absorption spectra and fluorescence spectra of the porphyrinic monomers and their corresponding polyimides were measured in dichloromethane (CH₂Cl₂) and N,N-dimethylacetamide (DMAc). The presence of PFMB and 6FDA units along the polymeric backbone causes the polymers to have moderate to high solubility in organic polar solvents. Fig. 8 shows the UV–Visible absorption spectra of the porphyrin monomers and their respective polyimide series I–IV and Table 3 lists the absorption spectral maxima. It is seen that hardly any shifting in the absorption maxima was observed between both solvents and between the porphyrin monomers and their respective polyimides. A slight shift of ~5 nm in both the Soret and Q bands between TPP and *cis*- and *trans*-DATPP monomers was observed, implying a small degree of electron charge transfer due to the presence of the electron donating –NH₂ groups. For the case of the zinc metalated porphyrin monomers (ZnTPP, *cis*-ZnDATPP, and *trans*-ZnDATPP) and their respective polyimide series III and IV, a bathochromic (or red) shift of ~10 nm in both the Soret and Q bands in going from CH₂Cl₂ to DMAc was observed. This minor red shift is attributed to the difference in polarity between both solvents (DMAc being more polar than CH₂Cl₂). The Dimroth-Reichardt Empirical Scales of solvent polarity ($E_T(30)$) are reported to be 40.7 kcal mol⁻¹ (for CH₂Cl₂) and 42.9 kcal mol⁻¹ (for DMAc), respectively [36]. Furthermore, it was also found in each polyimide series I–IV that changing the weight % of the porphyrin monomer had no measurable effect on the absorption maxima locations.

The fluorescence spectra of the porphyrin monomers and their corresponding polymers were also measured in CH₂Cl₂ and DMAc. Fig. 9 shows the fluorescence spectra of the porphyrin monomers

and their respective polyimides and Table 4 lists the fluorescence spectral maxima. For the porphyrin monomers, a slight bathochromic shift between a λ range of 10–25 nm was observed for *cis*- and *trans*-DATPP and their zinc metalated analogues, *cis*- and *trans*-ZnDATPP in going from CH₂Cl₂ to DMAc.

3.2. Photophysical properties

Tables 5 and 6 list the photophysical properties of the porphyrin monomers and their respective polyimide series of compounds in dichloromethane and N,N-dimethylacetamide solutions, including the measured fluorescence quantum yields (Φ_f), fluorescence lifetimes (τ_f), radiative (k_f) and nonradiative (k_{nr}) decay rate constants for each compound, as defined by Eqs. (6) and (7). Also listed in Tables 5 and 6 are the values for the electron transfer rate constant (k_{ET}) for each compound.

$$k_f = \frac{\Phi_f}{\tau_f} \quad (6)$$

$$k_{nr} = \left(\frac{1}{\Phi_f} - 1 \right) k_f \quad (7)$$

It was found that the free base porphyrin monomers and their corresponding polyimides had higher Φ_f and τ_f values than their zinc metalated derivatives. The lower Φ_f and τ_f values observed for the metalated derivatives are attributed to efficient singlet/triplet intersystem crossing in accordance to spin-orbit coupling and the heavy atom effect [37–39]. In spin-orbit coupling, the spin of an electron is affected by the angular momentum of its orbit. The matrix element for the spin-orbit coupling between the electronic wavefunctions $^1\Psi_n$ and $^3\Psi_m$ for states n and m, is expressed in Dirac notation by Eq. (8),

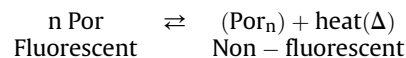
$$\langle ^1\Psi_n | \hat{H}_{SO} | ^3\Psi_m \rangle \quad (8)$$

where \hat{H}_{SO} is the spin-orbit coupling Hamiltonian operator that mixes the electronic states of different spin multiplicities. The spin-orbit coupling Hamiltonian operator, \hat{H}_{SO} , is defined by Eq. (9),

$$\hat{H}_{SO} = \sum_i \xi_{SO,i} \hat{L}_i \cdot \hat{S}_i \quad (9)$$

where ξ_{SO} is the spin-orbit coupling constant, related to the nuclear charge that the electron sees as it orbits the atoms in the molecule. The magnitude of ξ_{SO} is directly proportional to the fourth power of the atomic number (Z^4), in accordance to the heavy atom effect [37]. \hat{L} and \hat{S} are the operators for an electron's orbital angular momentum and spin angular momentum, respectively [38].

It was also found within each polyimide series (C1–C4, T1–T4, ZnC1–ZnC4, ZnT1–ZnT4) that Φ_f decreased with respect to an increase in the porphyrin content weight %. This decrease in Φ_f in going from 5 wt % to 30 wt % porphyrin could potentially be due to self-quenching, which, in the case of these class of organic compounds, occurs when an excited state of the porphyrin containing molecule exchanges energy with the same molecule in the ground state, resulting in the loss of heat through thermal dissipation, and therefore in the reduction of fluorescence. Self-quenching is represented by the following reversible reaction



Another interesting observation for each polyimide series is that in going from 5 wt % to 30 wt % porphyrin, Φ_f decreases and the

Table 2

Volumes and molar concentrations of 9,10-anthraquinone (AQ) for the 5 mL aliquot solutions.

Flask Number	Volume of AQ (mL)	[AQ] (M)
1	0	0
2	0.2	2.0×10^{-4}
3	0.4	4.0×10^{-4}
4	0.6	6.0×10^{-4}
5	0.8	8.0×10^{-4}
6	1.0	1.0×10^{-3}
7	1.2	1.2×10^{-3}
8	1.4	1.4×10^{-3}

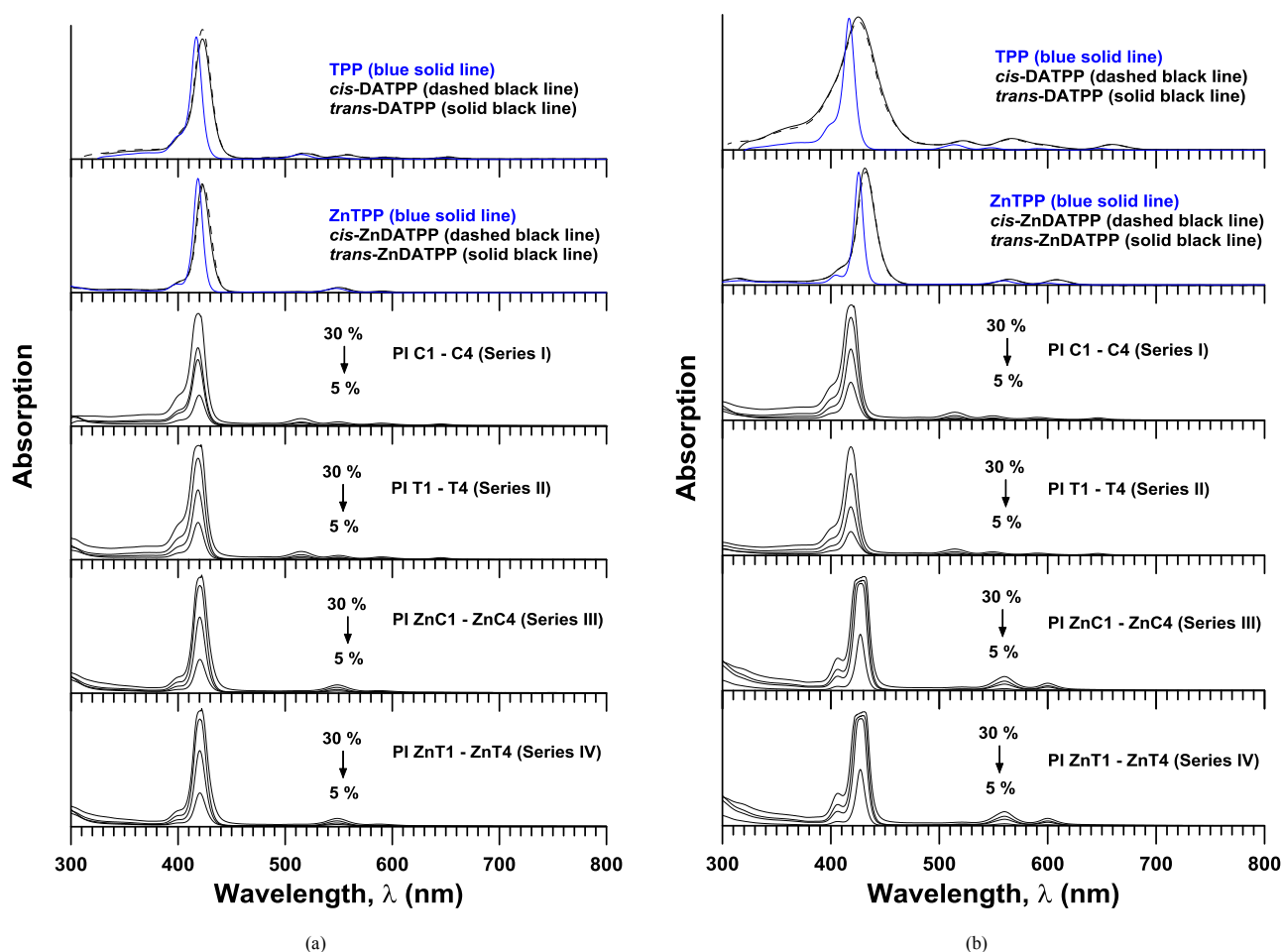


Fig. 8. UV-Visible absorption spectra of the porphyrin monomers and their corresponding polyimides series I–IV in (a) dichloromethane and (b) N,N-dimethylacetamide.

electron transfer rate constant (k_{ET}) increases. In reference to the structure of the porphyrin polyimide compounds (see Fig. 7), photoinduced intramolecular electron transfer occurs from the electron (π) donor porphyrin end to the electron (π) acceptor diimide end of the molecule. The electron transfer rate constants in both solvents have been found to increase with respect to an increase in the number of porphyrin groups in the polymer structure. Shown in Fig. 10 are plots of k_{ET} versus Φ_f for (a) free base polyimide series and (b) zinc metalated polyimide series in dichloromethane and N,N-dimethylacetamide. As shown in Fig. 10a, a linear inverse relationship was observed between Φ_f and k_{ET} for the free base polyimides (Series I and II, respectively). In the metalloporphyrin derivative compounds (Series III and IV, respectively), no linear relationship between Φ_f and k_{ET} was found. The k_{ET} values were found to be an order of magnitude larger than their corresponding free base polyimides. The larger k_{ET} values for the metalloporphyrin polyimide derivatives are perhaps due to the easier distribution of electronic charge from the electron donor end to the electron acceptor end.

3.3. Fluorescence quenching

Fluorescence quenching measurements were observed by the Stern-Volmer relationship (see Eq. (4)), using 9,10-anthraquinone (AQ) as the quencher molecule. From the Stern-Volmer relationship, the Stern-Volmer constant (K_Q) and the bimolecular quenching rate constant (k_q) were measured for each porphyrin/

AQ/solvent system (see Tables 7 and 8). Fig. 11 shows the Stern-Volmer plots for the fluorescence quenching of TPP, *cis*-DATPP, and *trans*-DATPP by AQ in dichloromethane and N,N-dimethylacetamide, together with corresponding fluorescence spectra in dichloromethane. It is clearly shown in each case that the fluorescence intensity decreases with respect to an increase in the concentration of AQ and a linear relationship between the ratio of the fluorescence intensities in the absence and presence of AQ and concentration of AQ were observed in the Stern-Volmer plots. The K_Q values were determined from the slopes of the Stern-Volmer plots and were found to range between 146–170 M^{-1} in CH_2Cl_2 and 96–126 M^{-1} in DMAc. The bimolecular quenching rate constant, k_q , was calculated upon knowledge of both K_Q and τ_f . The k_q values for TPP, *cis*-DATPP, and *trans*-DATPP were found to be 1.59×10^{10} , 1.95×10^{10} , $2.11 \times 10^{10} M^{-1} s^{-1}$ in CH_2Cl_2 and 8.00×10^9 , 2.56×10^{10} , $2.36 \times 10^{10} M^{-1} s^{-1}$ in DMAc, respectively. Results suggest that the relative magnitudes of k_q increase from TPP to both *cis*- and *trans*-DATPP due to the presence of electron donating diamino groups covalently bonded on the porphyrin moiety. The k_q values of the porphyrin/AQ/solvent systems are close to the diffusion coefficients of both solvents: $1.57 \times 10^{10} M^{-1} s^{-1}$ for dichloromethane and $3.32 \times 10^9 M^{-1} s^{-1}$ for N,N-dimethylacetamide, respectively. This indicates that molecular diffusion is a primary mechanism involved in the fluorescence quenching of the porphyrinic systems by AQ.

Similarly, the k_q values of the metalloporphyrin monomers, ZnTPP, *cis*-ZnDATPP, and *trans*-ZnDATPP were calculated to be

Table 3
UV–Visible absorption maxima of the porphyrin monomers and polyimide series I – IV.

Compound	Porphyrin Monomers			
	CH ₂ Cl ₂		DMAc	
	Soret band (nm)	Q-band (nm)	Soret band (nm)	Q-band (nm)
TPP	417	514, 549, 590, 644	417	514, 546, 589, 646
<i>cis</i> -DATPP	422	519, 555, 593, 650	424	520, 566, 599, 657
<i>trans</i> -DATPP	422	519, 555, 593, 650	424	520, 566, 598, 658
ZnTPP	419	548, 587	426	560, 600
<i>cis</i> -ZnDATPP	424	551, 592	434	564, 609
<i>trans</i> -ZnDATPP	424	551, 591	434	564, 610
Polyimide Series I–IV				
Series I (from <i>cis</i> -DATPP)				
PI-C1	418	514, 550, 590, 646	419	515, 549, 590, 645
PI-C2	418	514, 550, 590, 645	419	515, 550, 591, 646
PI-C3	418	514, 550, 590, 646	419	515, 550, 590, 646
PI-C4	418	514, 550, 590, 646	419	514, 550, 591, 646
Series II (from <i>trans</i> -DATPP)				
PI-T1	418	515, 550, 590, 646	419	515, 550, 591, 646
PI-T2	418	515, 550, 590, 645	419	515, 550, 591, 646
PI-T3	418	515, 550, 590, 646	419	515, 550, 591, 646
PI-T4	418	515, 550, 590, 646	419	515, 550, 591, 646
Series III (from <i>cis</i> -ZnDATPP)				
PI-ZnC1	420	549, 588	428	560, 600
PI-ZnC2	420	549, 588	429	560, 600
PI-ZnC3	421	549, 588	429	560, 600
PI-ZnC4	421	549, 588	429	560, 600
Series IV (from <i>trans</i> -ZnDATPP)				
PI-ZnT1	421	549, 590	428	560, 600
PI-ZnT2	420	549, 590	428	560, 600
PI-ZnT3	421	549, 589	429	560, 600
PI-ZnT4	421	549, 589	429	560, 600

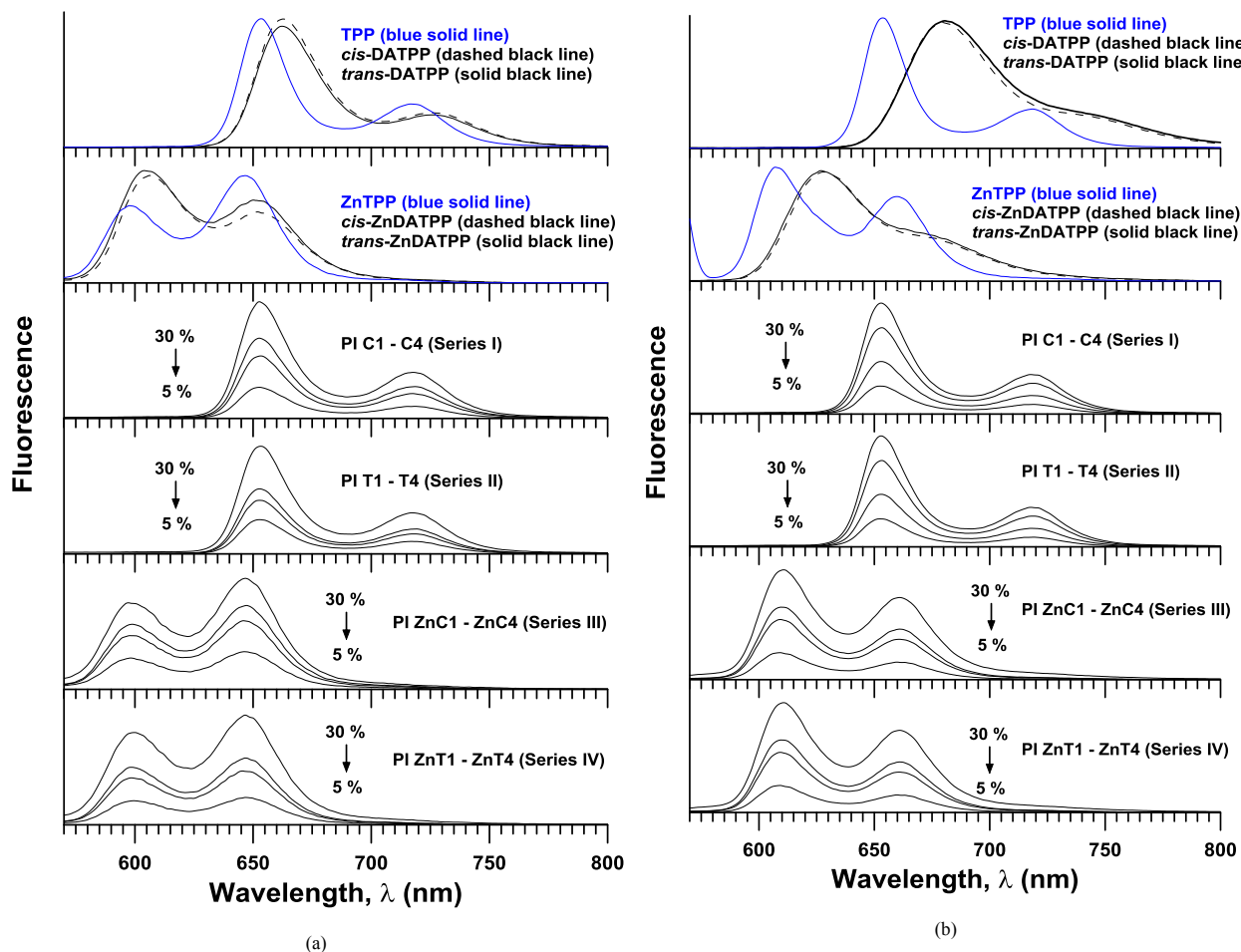


Fig. 9. Fluorescence spectra of the porphyrin monomers and their corresponding polyimide series I–IV in (a) dichloromethane and (b) N,N-dimethylacetamide.

Table 4
Fluorescence maxima of the porphyrin monomers and polyimide series I – IV.

Porphyrin Monomers		
Compound	CH ₂ Cl ₂	DMAc
	λ (nm)	λ (nm)
TPP	654, 718	654, 719
<i>cis</i> -DATPP	663, 724	680, 750
<i>trans</i> -DATPP	663, 725	680, 750
ZnTPP	599, 647	609, 660
<i>cis</i> -ZnDATPP	604, 650	628, 673
<i>trans</i> -ZnDATPP	604, 650	628, 673
Polyimide Series I–IV		
Series I (from <i>cis</i> -DATPP)		
PI-C1	653, 718	653, 718
PI-C2	653, 718	653, 719
PI-C3	653, 718	653, 719
PI-C4	653, 718	653, 719
Series II (from <i>trans</i> -DATPP)		
PI-T1	654, 718	653, 719
PI-T2	654, 718	653, 718
PI-T3	653, 718	653, 719
PI-T4	653, 718	653, 719
Series III (from <i>cis</i> -ZnDATPP)		
PI-ZnC1	599, 647	609, 661
PI-ZnC2	600, 647	609, 661
PI-ZnC3	600, 647	610, 661
PI-ZnC4	599, 647	610, 661
Series IV (from <i>trans</i> -ZnDATPP)		
PI-ZnT1	600, 647	609, 660
PI-ZnT2	599, 647	609, 661
PI-ZnT3	599, 647	610, 661
PI-ZnT4	600, 647	610, 661

Table 5
Photophysical properties of the porphyrin monomers and their corresponding polyimide series I – IV in dichloromethane.

Porphyrin Monomers					
Compound	Φ _f	τ _r (ns)	k _f (s ⁻¹)	k _{nr} (s ⁻¹)	k _{ET} (s ⁻¹)
TPP	0.116	9.21	1.26 × 10 ⁷	9.60 × 10 ⁷	–
<i>cis</i> -DATPP	0.181	8.02	2.26 × 10 ⁷	1.02 × 10 ⁸	–
<i>trans</i> -DATPP	0.171	8.06	2.12 × 10 ⁷	1.03 × 10 ⁸	–
ZnTPP	0.025	1.97	1.27 × 10 ⁷	4.95 × 10 ⁸	–
<i>cis</i> -ZnDATPP	0.029	1.55	1.87 × 10 ⁷	6.26 × 10 ⁸	–
<i>trans</i> -ZnDATPP	0.027	1.50	1.80 × 10 ⁷	6.49 × 10 ⁸	–
Polyimide Series I–IV					
Series I (from <i>cis</i> -DATPP)					
PI-C1	0.079	8.83	8.95 × 10 ⁶	1.04 × 10 ⁸	4.73 × 10 ⁶
PI-C2	0.070	8.47	8.26 × 10 ⁶	1.10 × 10 ⁸	9.45 × 10 ⁶
PI-C3	0.068	8.38	8.11 × 10 ⁶	1.11 × 10 ⁸	1.07 × 10 ⁷
PI-C4	0.054	8.09	6.67 × 10 ⁶	1.17 × 10 ⁸	1.50 × 10 ⁷
Series II (from <i>trans</i> -DATPP)					
PI-T1	0.076	8.65	8.79 × 10 ⁶	1.07 × 10 ⁸	7.02 × 10 ⁶
PI-T2	0.063	8.51	7.40 × 10 ⁶	1.10 × 10 ⁸	8.96 × 10 ⁶
PI-T3	0.057	8.27	6.89 × 10 ⁶	1.14 × 10 ⁸	1.24 × 10 ⁷
PI-T4	0.049	8.11	6.04 × 10 ⁶	1.17 × 10 ⁸	1.48 × 10 ⁷
Series III (from <i>cis</i> -ZnDATPP)					
PI-ZnC1	0.019	1.73	1.10 × 10 ⁷	5.67 × 10 ⁸	7.20 × 10 ⁷
PI-ZnC2	0.013	1.67	7.78 × 10 ⁶	5.91 × 10 ⁸	9.18 × 10 ⁷
PI-ZnC3	0.012	1.65	7.27 × 10 ⁶	5.99 × 10 ⁸	9.72 × 10 ⁷
PI-ZnC4	0.010	1.67	5.99 × 10 ⁶	5.93 × 10 ⁸	9.25 × 10 ⁷
Series IV (from <i>trans</i> -ZnDATPP)					
PI-ZnT1	0.018	1.75	1.03 × 10 ⁷	5.61 × 10 ⁸	6.54 × 10 ⁷
PI-ZnT2	0.012	1.66	7.23 × 10 ⁶	5.95 × 10 ⁸	9.43 × 10 ⁷
PI-ZnT3	0.011	1.67	6.59 × 10 ⁶	5.92 × 10 ⁸	9.11 × 10 ⁷
PI-ZnT4	0.009	1.68	5.36 × 10 ⁶	5.90 × 10 ⁸	8.90 × 10 ⁷

4.72 × 10¹⁰, 7.62 × 10¹⁰, and 8.25 × 10¹⁰ M⁻¹ s⁻¹ in dichloromethane, and 3.19 × 10⁹, 4.94 × 10¹⁰, and 5.39 × 10¹⁰ M⁻¹ s⁻¹ in N,N-dimethylacetamide, respectively. This also implies that

Table 6
Photophysical properties of the porphyrin monomers and their corresponding polyimide series I – IV in N,N-dimethylacetamide.

Porphyrin Monomers					
Compound	Φ _f	τ _r (ns)	k _f (s ⁻¹)	k _{nr} (s ⁻¹)	k _{ET} (s ⁻¹)
TPP	0.150	11.94	1.26 × 10 ⁷	7.12 × 10 ⁷	–
<i>cis</i> -DATPP	0.196	4.43	4.42 × 10 ⁷	1.81 × 10 ⁸	–
<i>trans</i> -DATPP	0.198	4.93	4.02 × 10 ⁷	1.63 × 10 ⁸	–
ZnTPP	0.024	1.94	1.24 × 10 ⁷	5.03 × 10 ⁸	–
<i>cis</i> -ZnDATPP	0.044	1.90	2.32 × 10 ⁷	5.03 × 10 ⁸	–
<i>trans</i> -ZnDATPP	0.042	1.86	2.26 × 10 ⁷	5.15 × 10 ⁸	–
Polyimide Series I–IV					
Series I (from <i>cis</i> -DATPP)					
PI-C1	0.148	11.67	1.27 × 10 ⁷	7.30 × 10 ⁷	1.94 × 10 ⁶
PI-C2	0.128	11.50	1.11 × 10 ⁷	7.58 × 10 ⁷	3.20 × 10 ⁶
PI-C3	0.108	11.32	9.54 × 10 ⁶	7.88 × 10 ⁷	4.59 × 10 ⁶
PI-C4	0.098	11.30	8.67 × 10 ⁶	7.98 × 10 ⁷	4.74 × 10 ⁶
Series II (from <i>trans</i> -DATPP)					
PI-T1	0.160	11.56	1.38 × 10 ⁷	7.27 × 10 ⁷	2.75 × 10 ⁶
PI-T2	0.129	11.40	1.13 × 10 ⁷	7.64 × 10 ⁷	3.97 × 10 ⁶
PI-T3	0.112	11.30	9.91 × 10 ⁶	7.86 × 10 ⁷	4.74 × 10 ⁶
PI-T4	0.084	11.17	7.52 × 10 ⁶	8.20 × 10 ⁷	5.77 × 10 ⁶
Series III (from <i>cis</i> -ZnDATPP)					
PI-ZnC1	0.018	1.80	1.10 × 10 ⁷	5.46 × 10 ⁸	4.13 × 10 ⁷
PI-ZnC2	0.013	1.78	7.30 × 10 ⁶	5.54 × 10 ⁸	4.54 × 10 ⁷
PI-ZnC3	0.011	1.78	6.18 × 10 ⁶	5.56 × 10 ⁸	4.73 × 10 ⁷
PI-ZnC4	0.010	1.78	5.62 × 10 ⁶	5.56 × 10 ⁸	4.54 × 10 ⁷
Series IV (from <i>trans</i> -ZnDATPP)					
PI-ZnT1	0.017	1.78	9.55 × 10 ⁶	5.52 × 10 ⁸	4.63 × 10 ⁷
PI-ZnT2	0.012	1.77	6.78 × 10 ⁶	5.58 × 10 ⁸	4.95 × 10 ⁷
PI-ZnT3	0.011	1.78	6.18 × 10 ⁶	5.56 × 10 ⁸	4.60 × 10 ⁷
PI-ZnT4	0.010	1.77	5.65 × 10 ⁶	5.59 × 10 ⁸	5.05 × 10 ⁷

diffusion is involved in the fluorescence quenching mechanism. The high k_q values observed for the set of metalloporphyrin monomers could also be due to the effects of heavy atom quenching [40].

For polyimide series I and II, the values of both K_Q and k_q decreased more significantly in both solvents from 5% to 30% porphyrin content when compared to their zinc metalated analogues (series III and IV). For series I, in dichloromethane, K_Q decreased 65.2% from 252.24 M⁻¹ (5%) to 87.71 M⁻¹ (30%); in N,N-dimethylacetamide, K_Q decreased 36.1% from 76.00 M⁻¹ (5%) to 48.56 M⁻¹ (30%). For series II, in dichloromethane, K_Q decreased 62.4% from 273.67 M⁻¹ (5%) to 102.92 M⁻¹ (30%); in N,N-dimethylacetamide, K_Q decreased 43.0% from 90.06 M⁻¹ (5%) to 51.30 M⁻¹ (30%). It is also observed that the k_q values of the polyimide series I and II are one order of magnitude greater in dichloromethane than in N,N-dimethylacetamide, attributing this to more rapid fluorescence quenching of the polyimide by AQ in less polar media.

The higher magnitudes of both the K_Q and k_q values in the 5 wt % than in the 30 wt % porphyrin polymers in both solvents can be explained by the amount, or level, of aggregation within the polymer structures. In fluorescence quenching, the fluorescence intensity of the analyte is expected to be minimized due to the greater number of intermolecular collisions between the excited singlet state of the analyte and the quencher. As expected, the small wt % amount of porphyrin in the polymer backbone chain (i.e. 5%) dissolves in the solvent more freely due to less aggregation of the molecules (less chain packing means an increase in free volume and flexible linkages [41]). Hence, the presence of less intramolecular polymeric aggregation causes the quencher molecules to move more freely and collide more easily with the polyimide molecules. In contrast, the presence of a greater number of porphyrin molecules in the polymer backbone chain (i.e. 30%) increases the effect of intramolecular aggregation, thereby resulting in higher chain packing, less free volume, and less flexible linkages between the

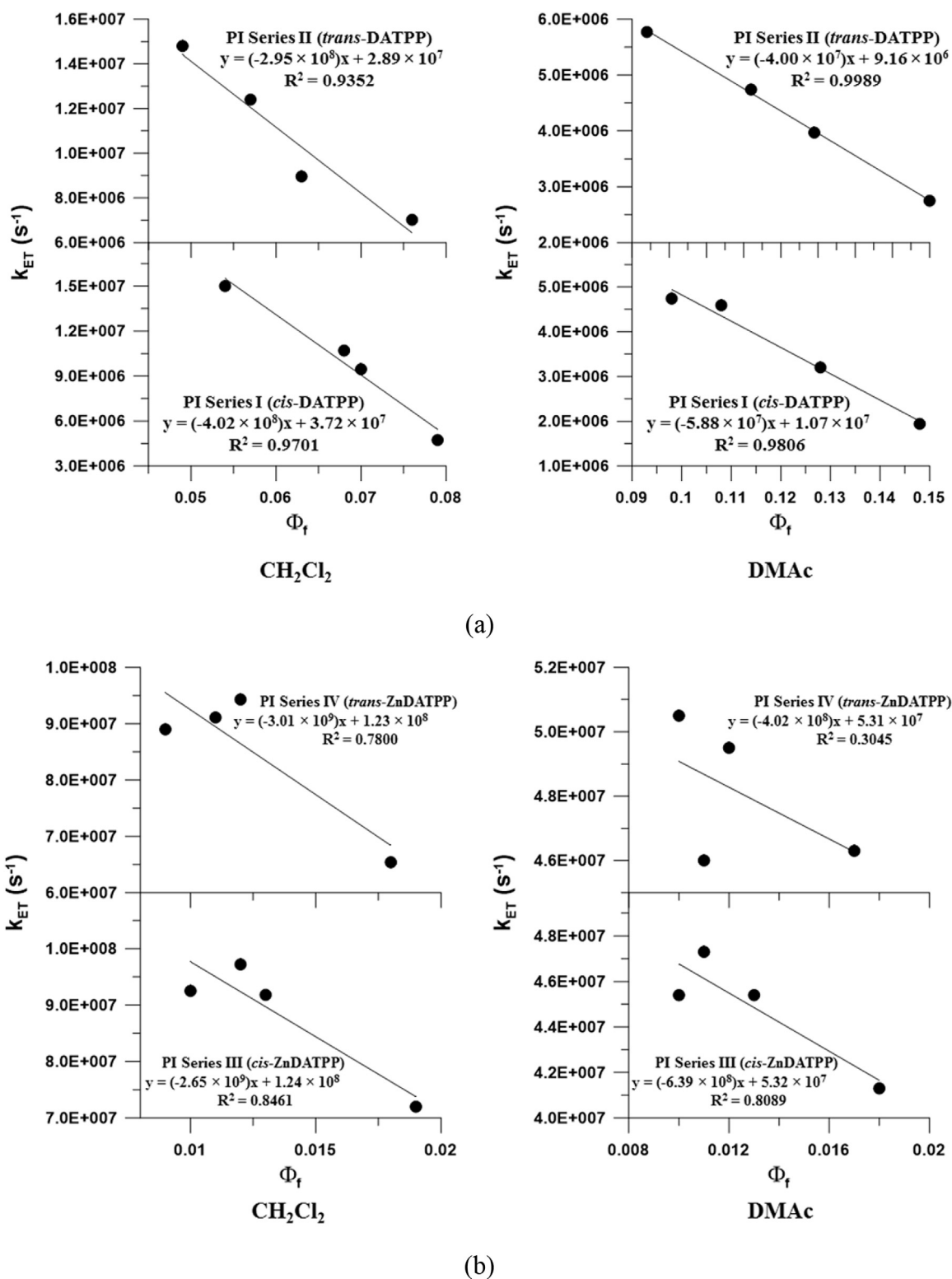


Fig. 10. Plots of k_{ET} versus Φ_f for (a) free base polyimide series and (b) zinc metalated polyimide series in dichloromethane (CH_2Cl_2) and N,N-dimethylacetamide (DMAc).

polyimide and quencher molecules. The cause of aggregation might serve to change the local environment that exists around the porphyrin macrocycle in the polyimide backbone chain, making it more difficult for the quencher to diffuse and interact within the interior of the polymer chain.

For the zinc metalloporphyrin polyimide derivatives (series III

and IV), both K_Q and k_q slightly decreased in going from 5 wt % to 30 wt % in both solvents. It is also observed that the magnitudes of k_q are greater than their corresponding free base polyimides. Both the small decrease in the magnitudes of K_Q and k_q and the higher magnitudes of k_q for the metalloporphyrin polyimide derivatives (series III and IV) are due to the heavy atom quenching effect [37].

The presence of zinc in the porphyrin macrocycle causes more of the excited singlet state molecules to undergo nonradiative singlet \rightarrow triplet intersystem crossing (higher k_{isc} and lower Φ_f), thereby resulting in a higher degree of fluorescence quenching.

Additional Stern-Volmer measurements consisted of examining the fluorescence quenching behavior of monomeric TPP and ZnTPP at a higher concentration range of AQ in both solvents. A fluorophore can simultaneously be quenched by intermolecular collisions with the quencher (process called dynamic quenching) or by ground-state complex formation with the quencher (process called static quenching). The characteristic feature of the Stern-Volmer plots in these circumstances is an upward curvature, concave toward the y-axis. The updated curving SV plots can be analyzed in terms of both the static and dynamic quenching constants (K_D and K_S , respectively). The fractional fluorescence intensity, F_0/F , is given by the product of static and dynamic quenching, defined as

$$\frac{F_0}{F} = (1 + K_D[Q])(1 + K_S[Q]) \quad (10)$$

This modified form of the Stern-Volmer equation is second order in $[Q]$, which accounts for the upward curvature observed when both static and dynamic quenching occur for the same fluorophore [32].

In the case of the fluorescence quenching of TPP and ZnTPP by AQ, the concentrations of TPP and ZnTPP remained constant at 5.0×10^{-6} M and the concentration of AQ ranged between 0.002 M and 0.016 M. Fig. 12 shows the Stern-Volmer plots for the fluorescence quenching of (a) TPP and (b) ZnTPP by AQ in dichloromethane and N,N-dimethylacetamide, together with their corresponding fluorescence spectra. As depicted, TPP and ZnTPP did not agree with the conventional Stern-Volmer linear relationship and the plot deviated from linearity at the higher concentrations of AQ, concaving upwards on the y-axis. The plot of the ratio of

Table 7

Calculated Stern-Volmer constants (K_Q) and bimolecular rate constants (k_q) for the fluorescence quenching of the porphyrin monomers and their corresponding polyimide series I – IV by 9,10-anthraquinone (AQ) in dichloromethane.

Porphyrin Monomers		
Compound	K_Q (M^{-1})	k_q ($M^{-1} s^{-1}$)
TPP	145.98	1.59×10^{10}
<i>cis</i> -DATPP	156.27	1.99×10^{10}
<i>trans</i> -DATPP	169.68	2.11×10^{10}
ZnTPP	93.03	4.72×10^{10}
<i>cis</i> -ZnDATPP	117.92	7.62×10^{10}
<i>trans</i> -ZnDATPP	124.01	8.25×10^{10}
Polyimide Series I–IV		
Series I (from <i>cis</i> -DATPP)		
PI-C1	252.24	2.86×10^{10}
PI-C2	134.77	1.59×10^{10}
PI-C3	116.96	1.40×10^{10}
PI-C4	87.71	1.08×10^{10}
Series II (from <i>trans</i> -DATPP)		
PI-T1	273.67	3.16×10^{10}
PI-T2	176.52	2.08×10^{10}
PI-T3	159.00	1.91×10^{10}
PI-T4	102.92	1.26×10^{10}
Series III (from <i>cis</i> -ZnDATPP)		
PI-ZnC1	83.32	4.83×10^{10}
PI-ZnC2	79.46	4.76×10^{10}
PI-ZnC3	85.52	5.17×10^{10}
PI-ZnC4	79.32	4.76×10^{10}
Series IV (from <i>trans</i> -ZnDATPP)		
PI-ZnT1	75.63	4.33×10^{10}
PI-ZnT2	70.26	4.23×10^{10}
PI-ZnT3	73.03	4.37×10^{10}
PI-ZnT4	73.13	4.36×10^{10}

Table 8

Calculated Stern-Volmer constants (K_Q) and bimolecular rate constants (k_q) for the fluorescence quenching of the porphyrin monomers and their corresponding polyimide series I – IV by 9,10-anthraquinone (AQ) in N,N-dimethylacetamide.

Porphyrin Monomers		
Compound	K_Q (M^{-1})	k_q ($M^{-1} s^{-1}$)
TPP	95.56	8.00×10^9
<i>cis</i> -DATPP	126.19	2.56×10^{10}
<i>trans</i> -DATPP	116.37	2.36×10^{10}
ZnTPP	61.97	3.19×10^{10}
<i>cis</i> -ZnDATPP	93.66	4.94×10^{10}
<i>trans</i> -ZnDATPP	100.34	5.39×10^{10}
Polyimide Series I–IV		
Series I (from <i>cis</i> -DATPP)		
PI-C1	76.00	6.51×10^9
PI-C2	60.09	5.22×10^9
PI-C3	52.86	4.67×10^9
PI-C4	48.56	4.32×10^9
Series II (from <i>trans</i> -DATPP)		
PI-T1	90.06	7.79×10^9
PI-T2	66.70	5.85×10^9
PI-T3	63.85	5.65×10^9
PI-T4	51.30	4.59×10^9
Series III (from <i>cis</i> -ZnDATPP)		
PI-ZnC1	67.89	3.78×10^{10}
PI-ZnC2	61.02	3.42×10^{10}
PI-ZnC3	62.29	3.51×10^{10}
PI-ZnC4	57.66	3.23×10^{10}
Series IV (from <i>trans</i> -ZnDATPP)		
PI-ZnT1	82.20	4.62×10^{10}
PI-ZnT2	65.38	3.69×10^{10}
PI-ZnT3	64.71	3.63×10^{10}
PI-ZnT4	60.47	3.42×10^{10}

the fluorescence lifetimes of TPP and ZnTPP both in the absence and presence of AQ against the concentration of AQ is also shown on the same plot. According to the Stern-Volmer plots depicted in Fig. 12, the positive nonlinear deviation indicates the simultaneous presence of dynamic and static quenching for the same fluorophore; that is, the fluorophore of interest (F) is quenched by (1) intermolecular collisions between the excited state fluorophore molecules and quencher (Q) and (2) ground state complex formation between the fluorophore and quencher (see Fig. 13).

From the fluorescence quenching data of TPP and ZnTPP by high concentrations of AQ in both solvents, the static and dynamic quenching constants can be determined from a plot of the apparent quenching constant (K_{app}) versus the concentration of AQ. This plot yields a straight line with a slope of $K_D K_S$ and a y-intercept of $K_D + K_S$ (see Fig. 14). As shown in Fig. 14, these plots are found to be sufficiently linear, indicating the presence of the parallel static and dynamic quenching mechanisms.

The plot of τ_0/τ versus $[Q]$, also shown in Fig. 12 for each monomer gives a straight line with a slope equal to K_D . In dichloromethane, K_D is equal to $36.1 M^{-1}$ and $13.5 M^{-1}$ for TPP and ZnTPP, and in N,N-dimethylacetamide, K_D is equal to $12.4 M^{-1}$ and $21.9 M^{-1}$ for TPP and ZnTPP, respectively. From the K_D values, the static quenching constants (K_S) for each compound/solvent system are determined from the slope of the second order Stern-Volmer plot (Fig. 14), provided that the slope is equal to $K_D K_S$. In dichloromethane, the K_S values were calculated to be $101.3 M^{-1}$ and $169.9 M^{-1}$ for TPP and ZnTPP. In N,N-dimethylacetamide, K_S values were calculated to be $176.6 M^{-1}$ and $91.5 M^{-1}$ for TPP and ZnTPP, respectively.

Data shows that the static quenching component (K_S) is significantly larger than the dynamic quenching component (K_D), indicating a high rate of complex formation. The results suggest that the positive deviations from linearity in the Stern-Volmer plots of

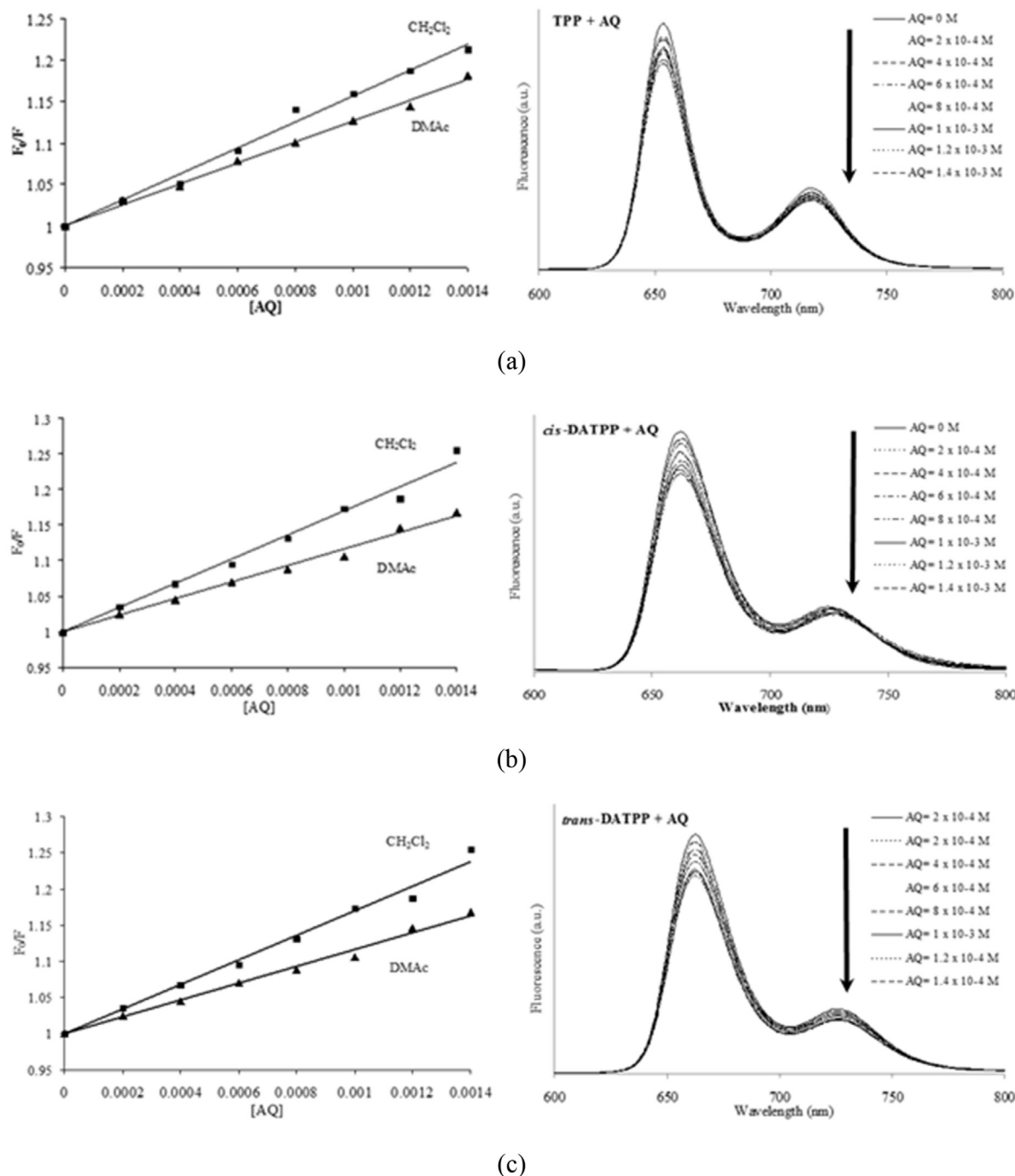


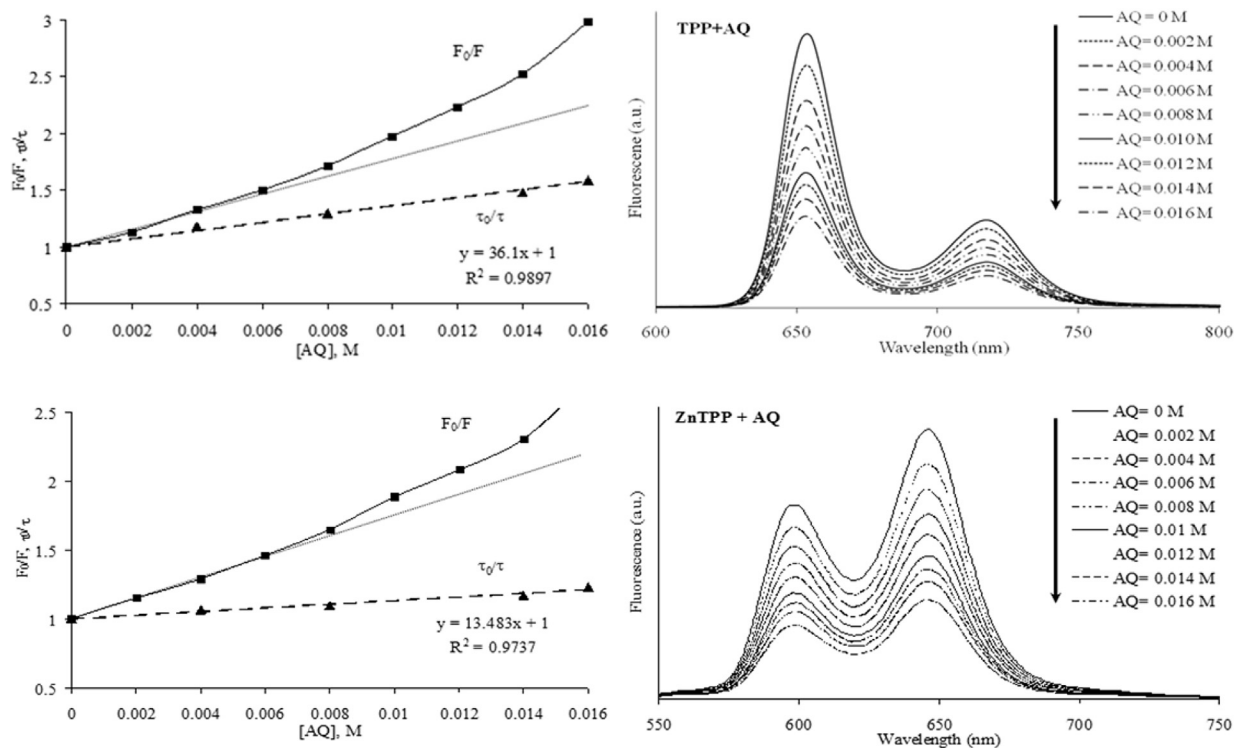
Fig. 11. Left: Stern-Volmer plots for the fluorescence quenching of (a) TPP, (b) *cis*-DATPP, and (c) *trans*-DATPP by 9,10-anthraquinone (AQ) in dichloromethane (CH_2Cl_2) and N,N-dimethylacetamide (DMAc). Right: Set of corresponding fluorescence spectra in dichloromethane.

TPP and ZnTPP in both solvents are due to the presence of a high static quenching component and ground state complex formation. Therefore, according to the results, static quenching and complex formation between the ground states of the fluorophore of interest and the quencher is the dominant mechanism of fluorescence quenching of these systems.

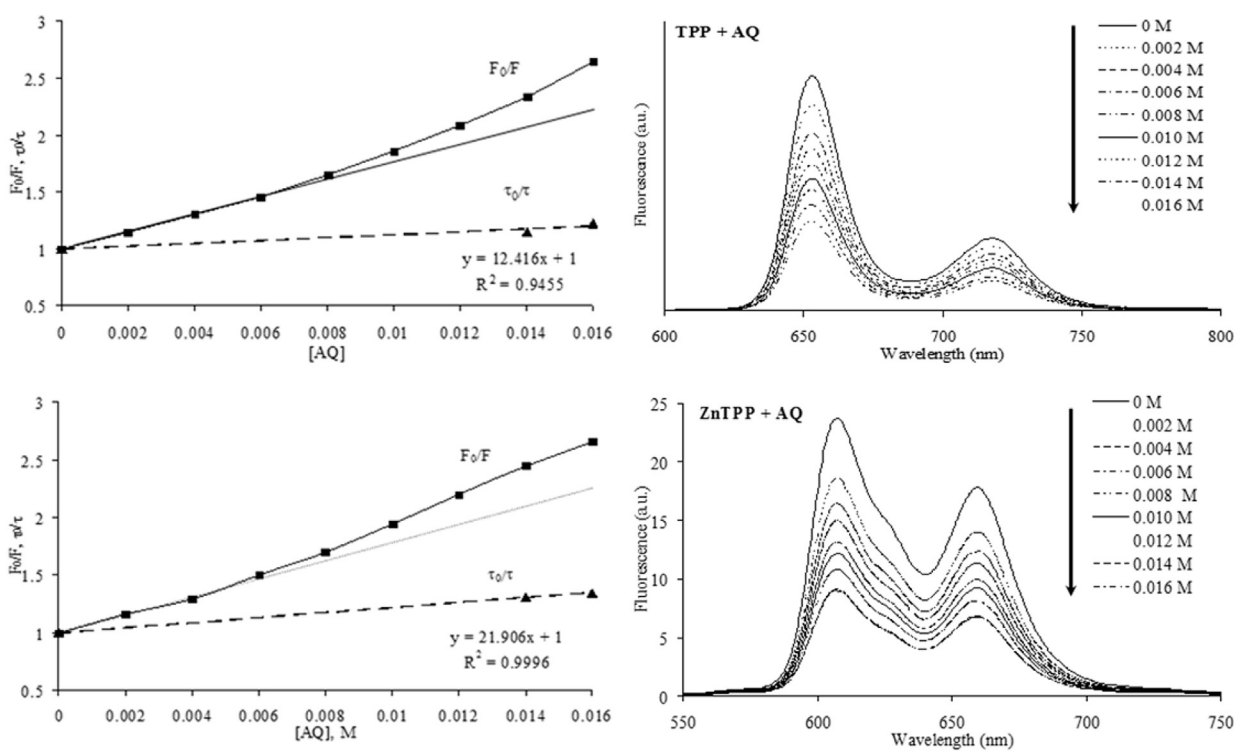
4. Conclusion

A series of free base and zinc metalated porphyrin monomers and their corresponding soluble polyimides with porphyrin weight

% content ranging between 5% and 30% were synthesized and structurally characterized. Spectroscopic and photophysical properties consisted of measuring UV–Visible absorption and fluorescence spectra, fluorescence quantum yields (Φ_f), and fluorescence lifetimes (τ_f) in dichloromethane and N,N-dimethylacetamide. Overall, minor red shifts in absorption and fluorescence approximately ranging between 5 and 25 nm were observed, attributing the shifts to electronic charge transfer and differences in solvent polarity. The free base porphyrin monomers and their corresponding polyimides had higher Φ_f and τ_f values than their zinc metalated analogues, attributing the lower values for the metalated



(a)



(b)

Fig. 12. Left: Stern-Volmer plots for the fluorescence quenching of TPP and ZnTPP by higher concentrations of 9,10-anthraquinone (AQ) in (a) dichloromethane and (b) N,N-dimethylacetamide. Right: Set of corresponding fluorescence spectra.

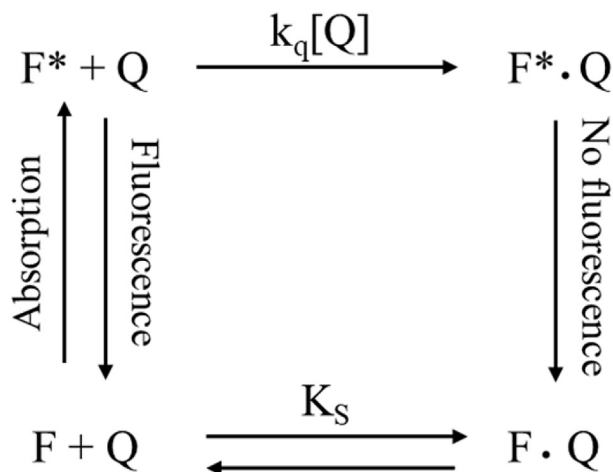


Fig. 13. Pathway of dynamic (collisional) quenching and static quenching [31].

analogues to efficient singlet/triplet intersystem crossing in accordance to spin-orbit coupling and the heavy atom effect. In each polyimide series (C1–C4, T1–T4, ZnC1–ZnC4, and ZnT1–ZnT4), Φ_f decreased and the electron transfer rate constant (k_{ET}) increased with respect to an increase in the porphyrin weight % content. The decrease in Φ_f in going from 5 wt % to 30 wt % is potentially due to self-quenching and the increase in k_{ET} is most likely due to photoinduced intramolecular electron transfer between the

electron (π) donor porphyrin end to the electron (π) acceptor diimide end of the molecule, in reference to the chemical structure of the polyimide.

Fluorescence quenching was measured and observed by the Stern-Volmer relationship, using 9,10-anthraquinone (AQ) acting as the quencher molecule. Both the Stern-Volmer constant (K_Q) and the bimolecular rate constant of fluorescence quenching (k_q) were calculated from the Stern-Volmer plots. For free base *cis*- and *trans*-DATPP and their zinc metalated analogues, *cis*- and *trans*-ZnDATPP, the calculated values of k_q are close to the diffusion coefficients of dichloromethane and *N,N*-dimethylacetamide. This indicates that molecular diffusion is a primary mechanism involved in fluorescence quenching. The high k_q values observed for the set of metalloporphyrin monomers could also be due to the effects of heavy atom quenching. The higher magnitudes of both the K_Q and k_q in the 5% than in the 30% porphyrin polyimides can be attributed to the amount, or level, of intramolecular polymeric aggregation. The level of aggregation might serve to change the local environment around the porphyrin macrocycle in the backbone chain, making it either easier or difficult for the quencher to diffuse and interact. Furthermore, positive deviations from nonlinearity at a higher range of quencher concentration indicates the simultaneous presence of dynamic (collisional) quenching and static quenching for the same fluorophore. The significantly larger values in the static quenching components (K_S) than in the dynamic quenching components (K_D) indicate that static quenching and ground state complex formation between the fluorophore and quencher is the dominant mechanism of fluorescence quenching of these systems

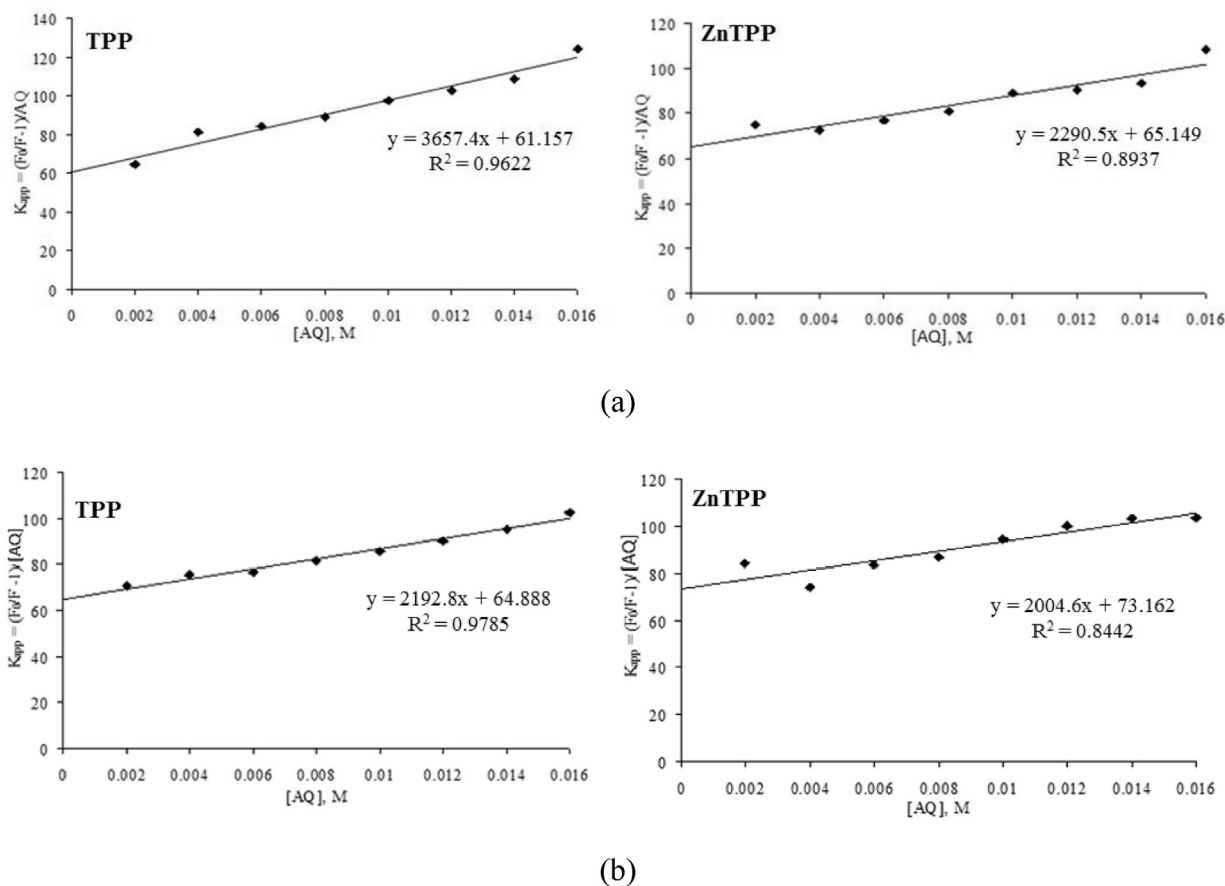


Fig. 14. Plot of the apparent quenching constant ($K_{app} = [(F_0/F) - 1]/[AQ]$) versus $[AQ]$ for the fluorescence quenching of TPP and ZnTPP by AQ in (a) dichloromethane and (b) *N,N*-dimethylacetamide.

at higher quencher concentrations. Furthermore, the work presented in this manuscript provides important information into the syntheses and photophysical properties of these classes of organic compounds. A thorough understanding of the properties of these compounds is relevant to studying their applications.

Appendix A. Supplementary data

Supplementary data related to this article can be found at <https://doi.org/10.1016/j.molstruc.2017.09.091>.

References

- [1] L.R. Milgrom, *The Colours of Life*, first ed., Oxford University Press, New York, 1997.
- [2] K.M. Smith, *Porphyryns and Metalloporphyryns*, first ed., Elsevier Scientific Publishing Company, Amsterdam, 1975.
- [3] R.J.P. Williams, *Chem. Rev.* 56 (1956) 299.
- [4] G.P. Gurinovich, A.N. Sevchenko, K.N. Solov'ev, *Sov. Phys. Usp.* 6 (1963) 67.
- [5] F.R. Longo, J.J. Leonard, J.B. Kim, *J. Am. Chem. Soc.* 94 (1972) 3986.
- [6] E.E. Bonfantini, A.K. Burrell, D.L. Officer, D.C.W. Reid, M.R. McDonald, P.A. Cocks, K.C. Gordon, *Inorg. Chem.* 36 (1997) 6270.
- [7] A. Ambroise, C. Kirmaier, R.W. Wagner, R.S. Loewe, D. Bocian, J.S. Lindsey, *J. Org. Chem.* 67 (2002) 3811.
- [8] C.-P. Jellen, H. Bettermann, *J. Mol. Struct.* 563–564 (2001) 119.
- [9] S. Tao, G. Li, H. Zhu, *J. Mater. Chem.* 16 (2006) 4521.
- [10] Z. Bao, L. Yu, *TRIP* 3 (1995) 159.
- [11] E.G. Azenha, A.C. Serra, M. Pineiro, M.M. Pereira, J. Seixas de Melo, L.G. Arnaut, S.J. Formosinho, A. M. d'A. Rocha Gonsalves, *Chem. Phys.* 280 (2002) 177.
- [12] M.C. DeRosa, R.J. Crutchley, *Coord. Chem. Rev.* 233–234 (2002) 351.
- [13] A. Toutchkine, E.L. Clennan, *Tetrahedron Lett.* 40 (1999) 6519.
- [14] C. Changtong, D.W. Carney, L. Luo, C.A. Zoto, J.L. Lombardi, R.E. Connors, *J. Photochem. Photobiol. A Chem.* 260 (2013) 9.
- [15] J.F. Lovell, J. Chen, M.T. Jarvi, W.-G. Cao, A.D. Allen, Y. Liu, T.T. Tidwell, B.C. Wilson, G. Zheng, *J. Phys. Chem. B* 113 (2009) 3203.
- [16] N.J. Turro, *Modern Molecular Photochemistry*, University Science Books, Sausalito, CA, 1991.
- [17] H.H. Wassermann, J.L. Ives, *Tetrahedron* 37 (1981) 1825.
- [18] D. Wilson, H.D. Stenzenberger, P.M. Hergenrother, *Polyimides*, Blackie & Son, Ltd., Glasgow & London: United Kingdom, 1990.
- [19] Y. Nishikata, A. Morikawa, M. Kakimoto, Y. Imai, K. Nishiyama, M. Fujihara, *Polym. J.* 22 (1990) 593.
- [20] Z.K. Xu, B.K. Zhu, Y.Y. Xu, *Chem. Mater.* 10 (1998) 1350.
- [21] B.K. Zhu, Z.K. Xu, Y.Y. Xu, *Eur. Polym. J.* 35 (1999) 77.
- [22] K. Takahashi, Y. Takano, T. Yamaguchi, J.I. Nakamura, C. Yokoe, K. Murata, *Synth. Met.* 155 (2005) 51.
- [23] K. Takechi, T. Shiga, T. Motohiro, T. Akiyama, S. Yamada, H. Nakayama, K. Kohama, *Sol. Energy Mater. Sol. Cells* 90 (2006) 1322.
- [24] U. Johanson, M. Marandi, V. Sammelselg, J. Tamm, *J. Electroanal. Chem.* 575 (2005) 267.
- [25] Z.N. Bao, Y.M. Chen, L.P. Yu, *Macromolecules* 27 (1994) 4629.
- [26] R.W. Wagner, J.S. Lindsey, *J. Am. Chem. Soc.* 116 (1994) 9759.
- [27] B.K. Zhu, Y.Y. Xu, X.Z. Wei, Z.K. Xu, *Polym. Int.* 53 (2004) 708.
- [28] M. Tomikawa, F.W. Harris, S.Z.D. Cheng, E. Galentier, *React. Funct. Polym.* 30 (1996) 101.
- [29] A.D. Adler, F.R. Longo, J.D. Finarelli, J. Goldmacher, J. Assour, L. Korsakoff, *J. Org. Chem.* 32 (1967) 476.
- [30] L. Raymond, J. Laurent, R. Frank, M. Fronczek, H.V. Graca, M.S. Kevin, *Tetrahedron* 60 (2004) 2757.
- [31] W. Anannarukan, S. Tantayanon, D. Zhang, E.A. Alemán, D.A. Modarelli, F.W. Harris, *Polymer* 47 (2006) 4936.
- [32] J.R. Lacowicz, *Principles of Fluorescence Spectroscopy*, second ed., Springer, New York, 2004.
- [33] A. Drzewiecka, K. Urbanska, Z. Matuszak, M. Pineiro, L.G. Arnaut, J. Habdas, A. Ratuszna, G. Stochel, *Acta Biochim. Pol.* 48 (2001) 277.
- [34] J.-P. Strachan, S. Gentemann, J. Seth, W.A. Kalsbeck, J.S. Lindsey, D. Holten, D.F. Bocian, *J. Am. Chem. Soc.* 119 (1997) 11191.
- [35] D.R. Lide, "Fluid Properties" in *CRC Handbook of Chemistry & Physics*, 77th edition, CRC Press, Boca Raton, FL, 1996–1997.
- [36] P. Suppan, N. Ghonheim, *Solvatochromism*, The Royal Society of Chemistry, United Kingdom, Cambridge, 1997.
- [37] J. Barltrop, J.D. Coyle, *Principles of Photochemistry*, Wiley & Sons, New York, 1978.
- [38] M.A. El-Sayed, *J. Chem. Phys.* 38 (1963) 2834.
- [39] N.J. Turro, V. Ramamurthy, J.C. Scaiano, *Principles of Molecular Photochemistry an Introduction*, University Science Books, Sausalito, CA, 2009.
- [40] E.G. Azenha, A.C. Serra, M. Pineiro, M.M. Pereira, J. Seixas de Melo, L.G. Arnaut, S.J. Formosinho, A. M. d'A. Rocha Gonsalves, *Chem. Phys.* 280 (2002) 177.
- [41] W. Anannarukan, *Synthesis of Polyimides Containing Tetrphenylporphyrin Moieties*, Ph. D. dissertation, Department of Chemistry, Chulalongkorn University, Bangkok, Thailand, 2003.